Electronic Supporting Information (ESI)

Use of Eugenol scaffold to Explore Explosive Sensing Properties of Cd(II) Based Coordination Polymers : Experimental Studies and Real Sample Analysis

Suvamoy Malik,[⊥,a] Udayan Mondal,[⊥,b,c] Narayan Ch. Jana,[d] Priyabrata Banerjee*[,b,c] and Amrita Saha,*[a]

[a] *Department of Chemistry, Jadavpur University, Kolkata- 700032, India.*

E-mail: amritasahachemju@gmail.com; amrita.saha@jadavpuruniversity.in;

[b] *Electric Mobility and Tribology Research Group, CSIR-Central Mechanical Engineering Research Institute, Durgapur, West Bengal 713209, India, Email: pr_banerjee@cmeri.res.in; Webpage: www.cmeri.res.in; www.priyabratabanerjee.in.*

[c] *Academy of Scientific and Innovative Research (AcSIR), Ghaziabad, Uttar Pradesh 201002, India*

[d] *School of Chemical Sciences, National Institute of Science Education and Research (NISER), Jatni, Khurda, Bhubaneswar, Odisha, PIN 752050, India.*

**Corresponding Authors*

[⊥] *contributed equally as first authors.*

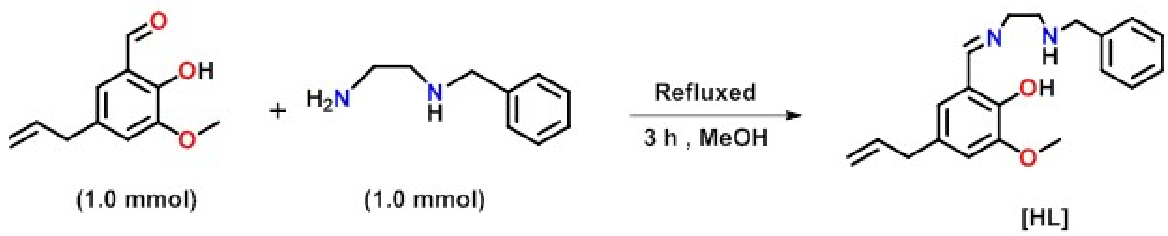

Scheme S1. Synthesis route of **HL**

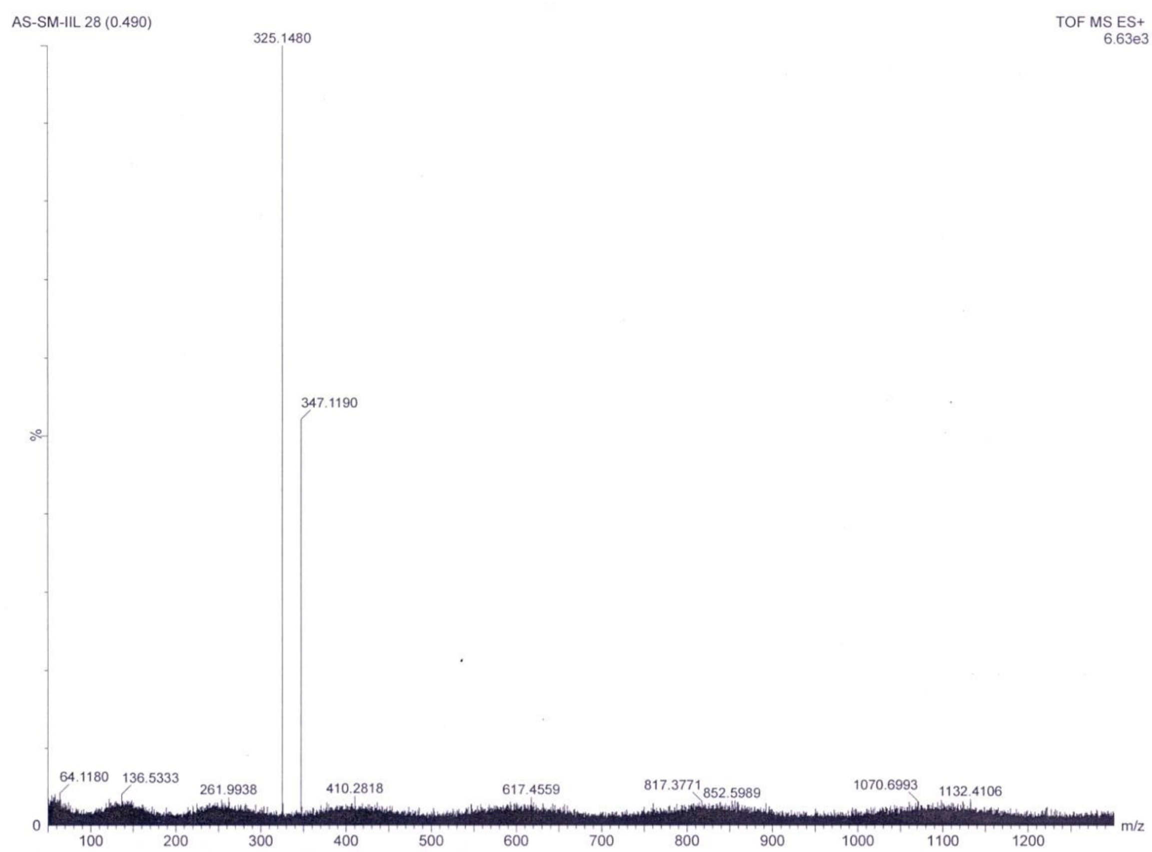

Fig. S1 ESI-mass spectrum of **HL** in CH_3OH solvent.

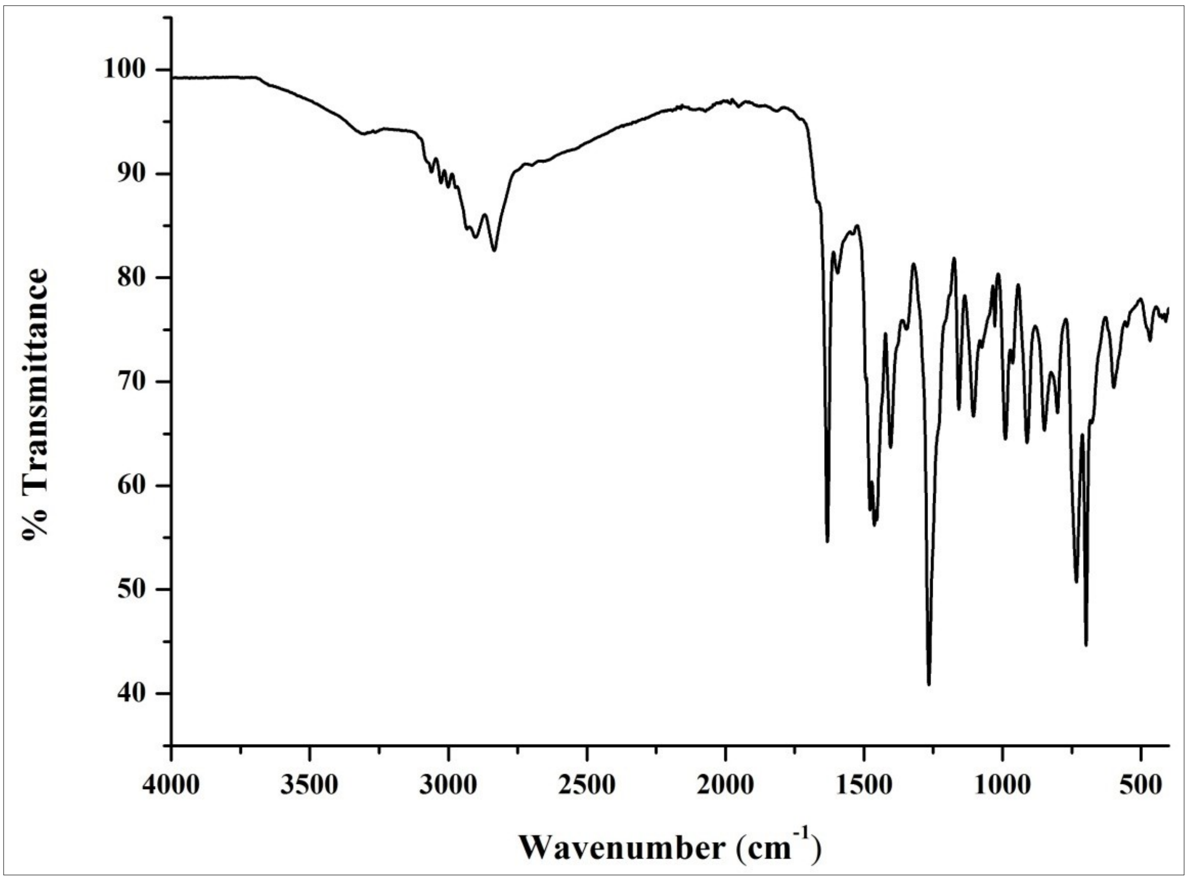

Fig. S2 IR spectrum of **HL**

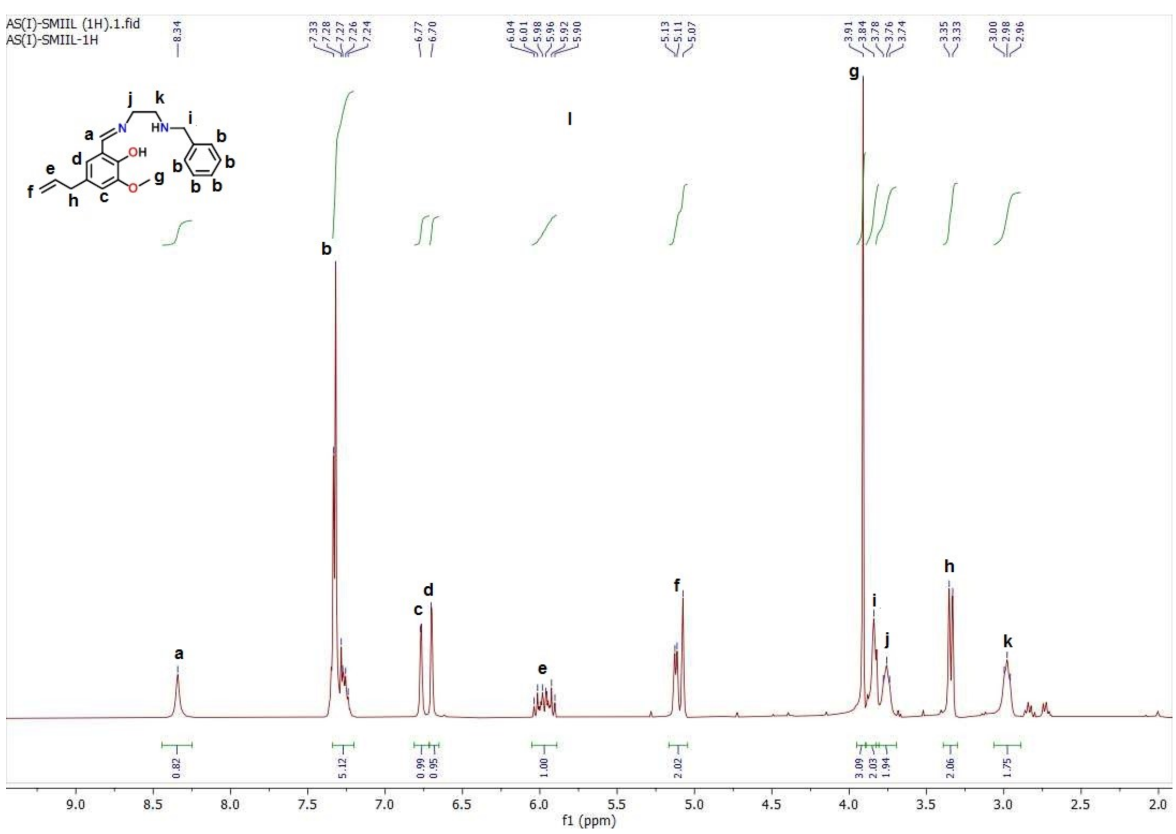

Fig. S3 ^{1}H NMR of **HL** in $CDCl_3$ solvent.

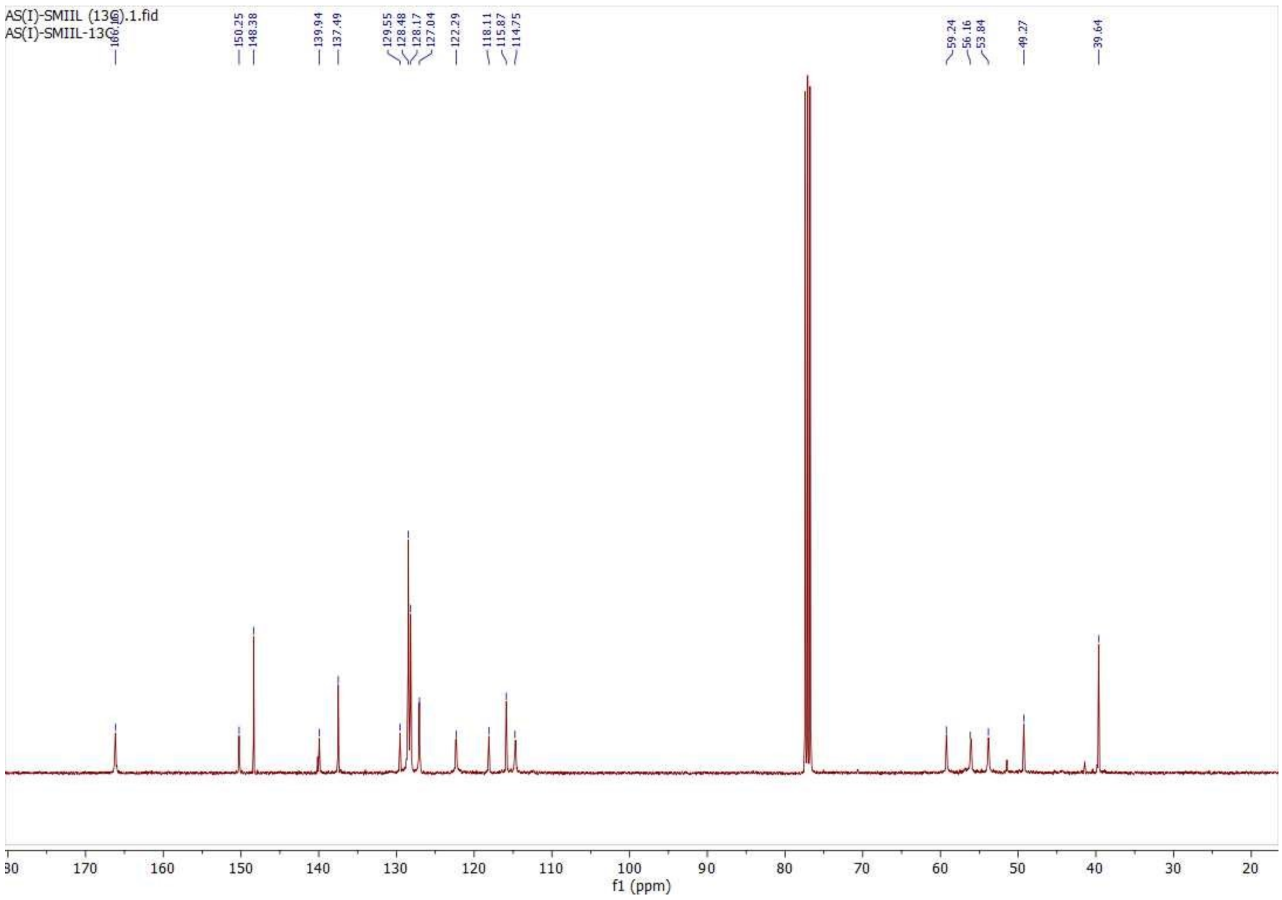

Fig. S4 ^{13}C NMR of **HL** in $CDCl_3$ solvent.

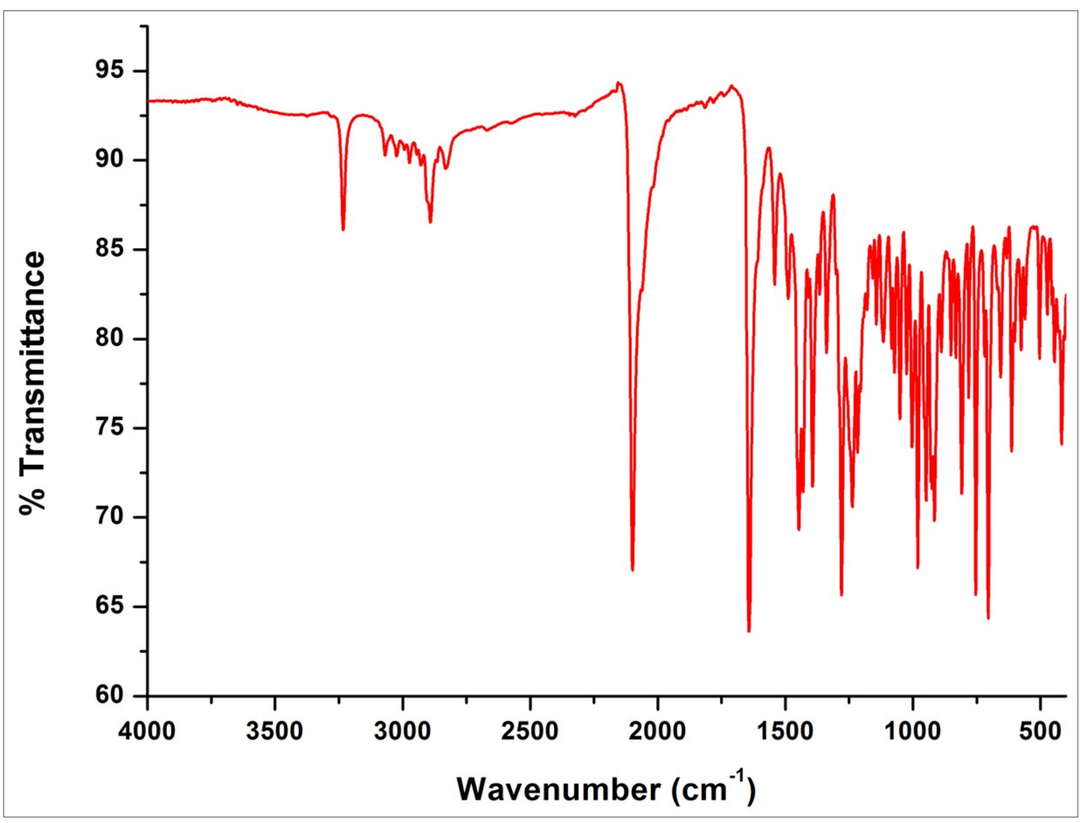

Fig. S5 IR spectrum of CP **1**

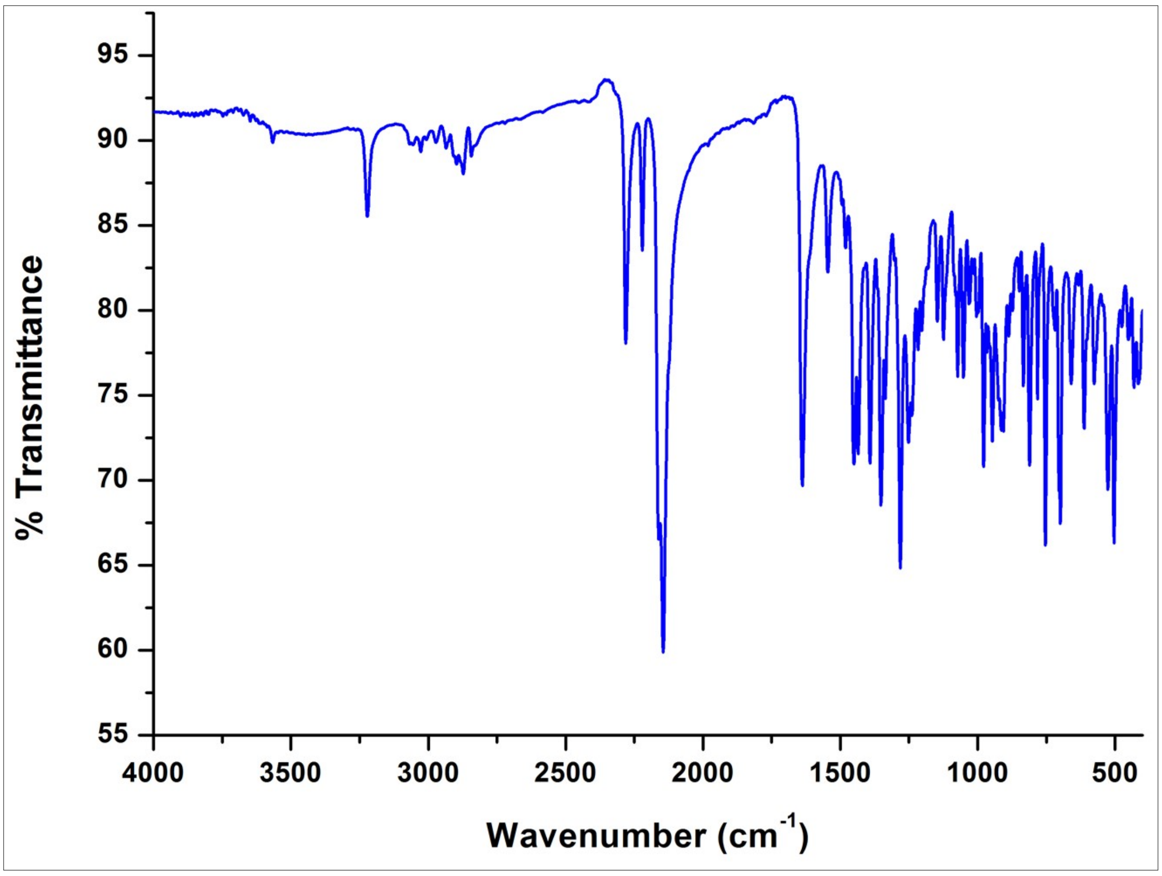

Fig. S6 IR spectrum of CP **2**

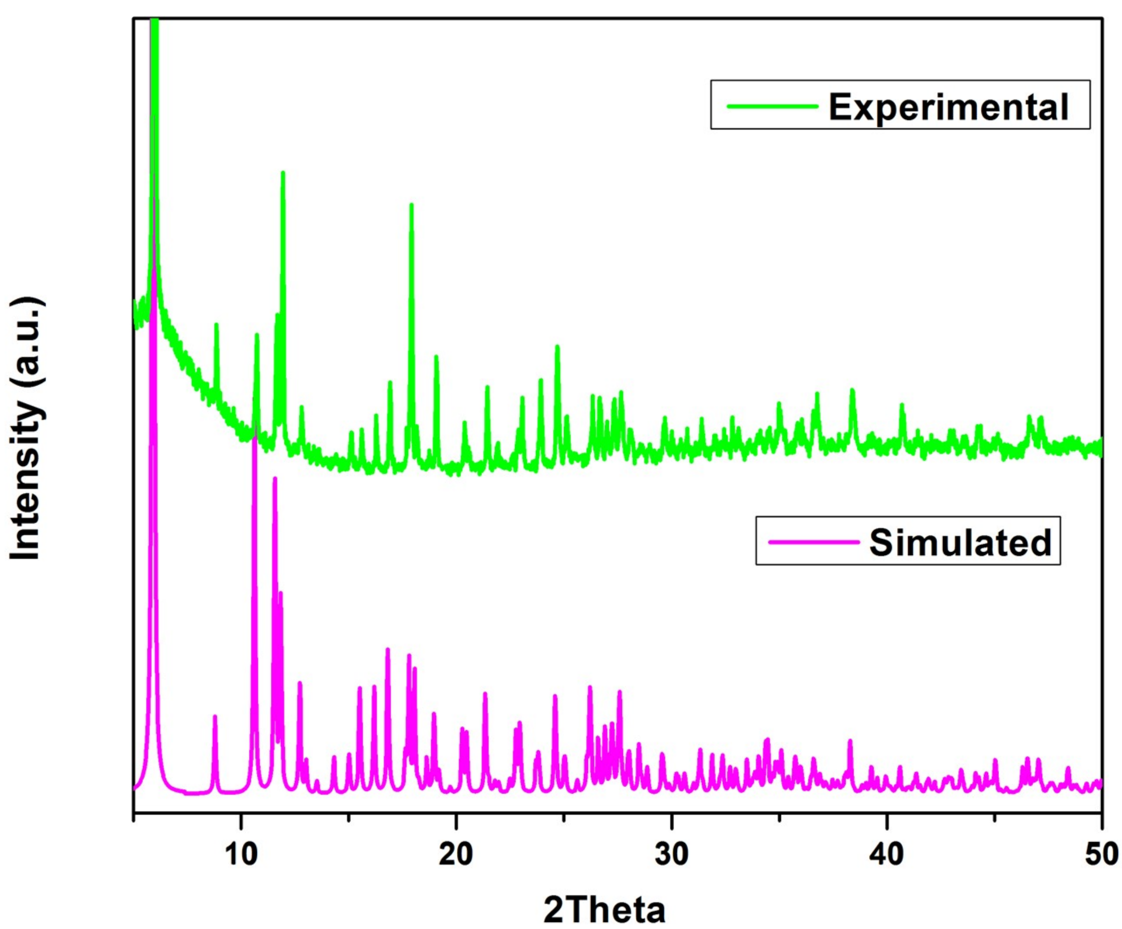

Fig. S7 Experimental and simulated PXRD pattern of **1**

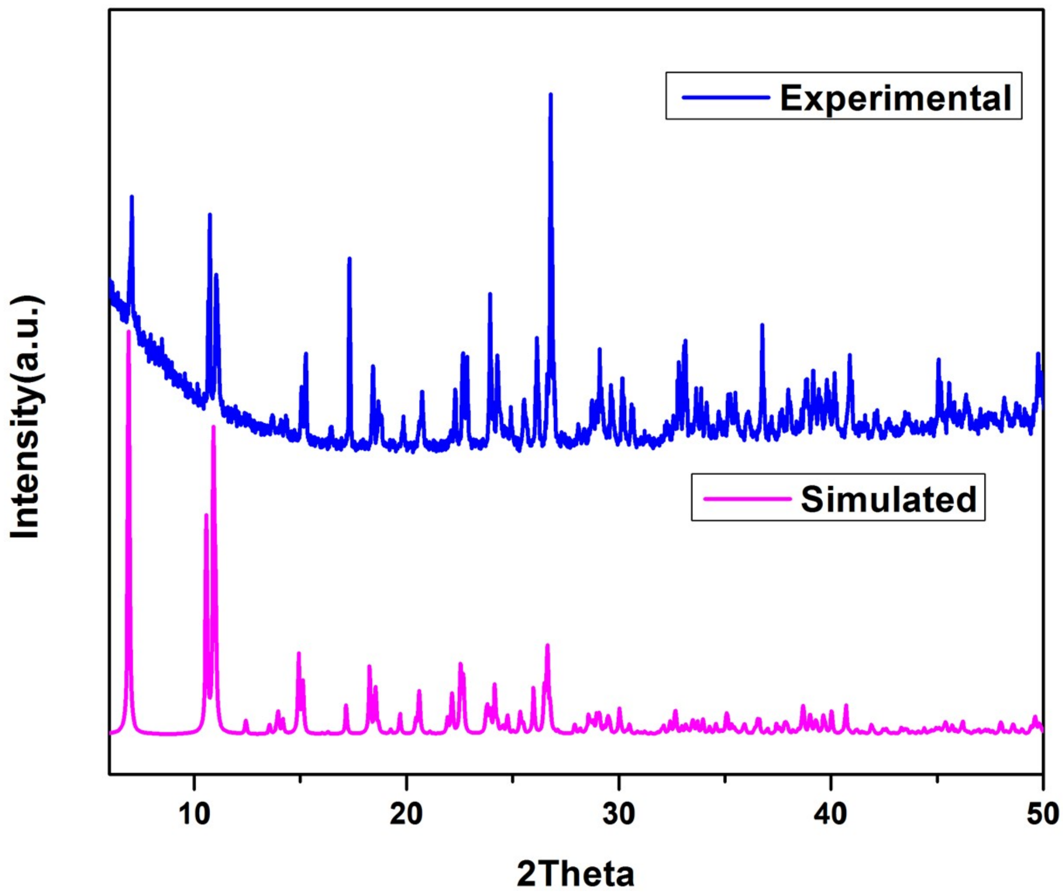

Fig. S8 Experimental and simulated PXRD pattern of **2**

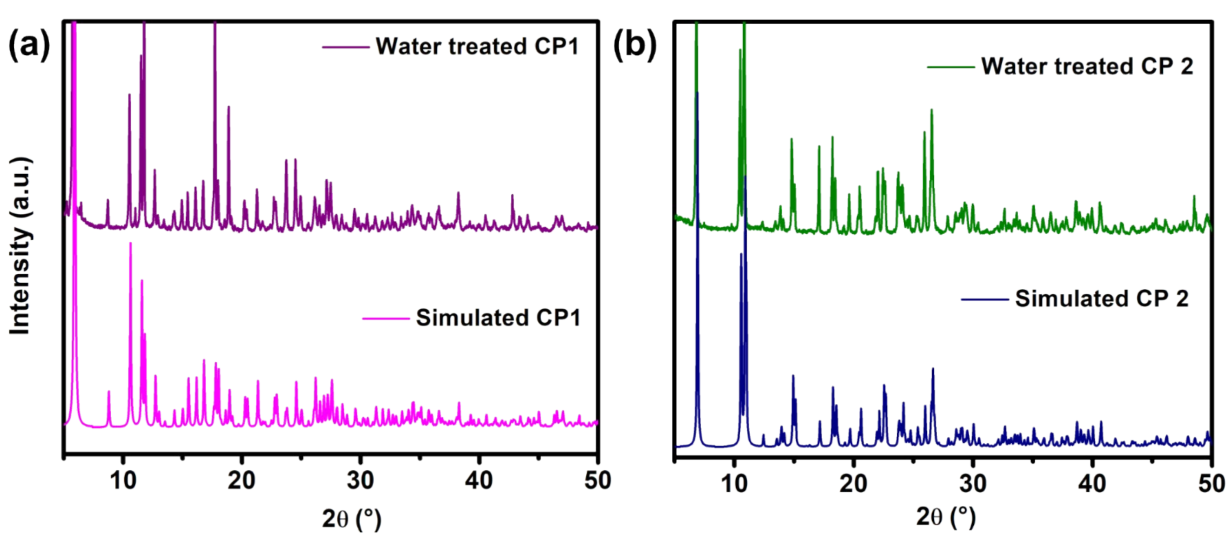

Fig. S9. Examining the water stability of the as-synthesized CPs (**1**, **2**) through PXRD.

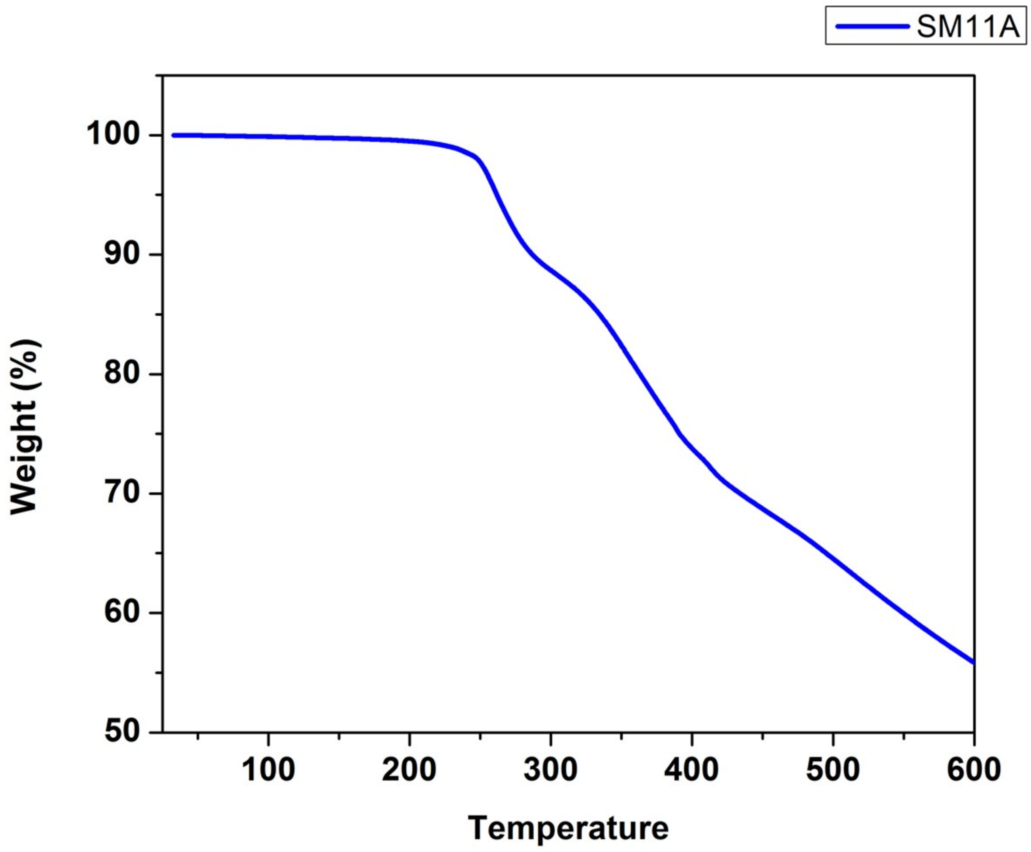

Fig. S10 Thermo Gravimetric Analysis of CP **1** under nitrogen atmosphere showing stability of complex is very appreciable up to 235ºC.

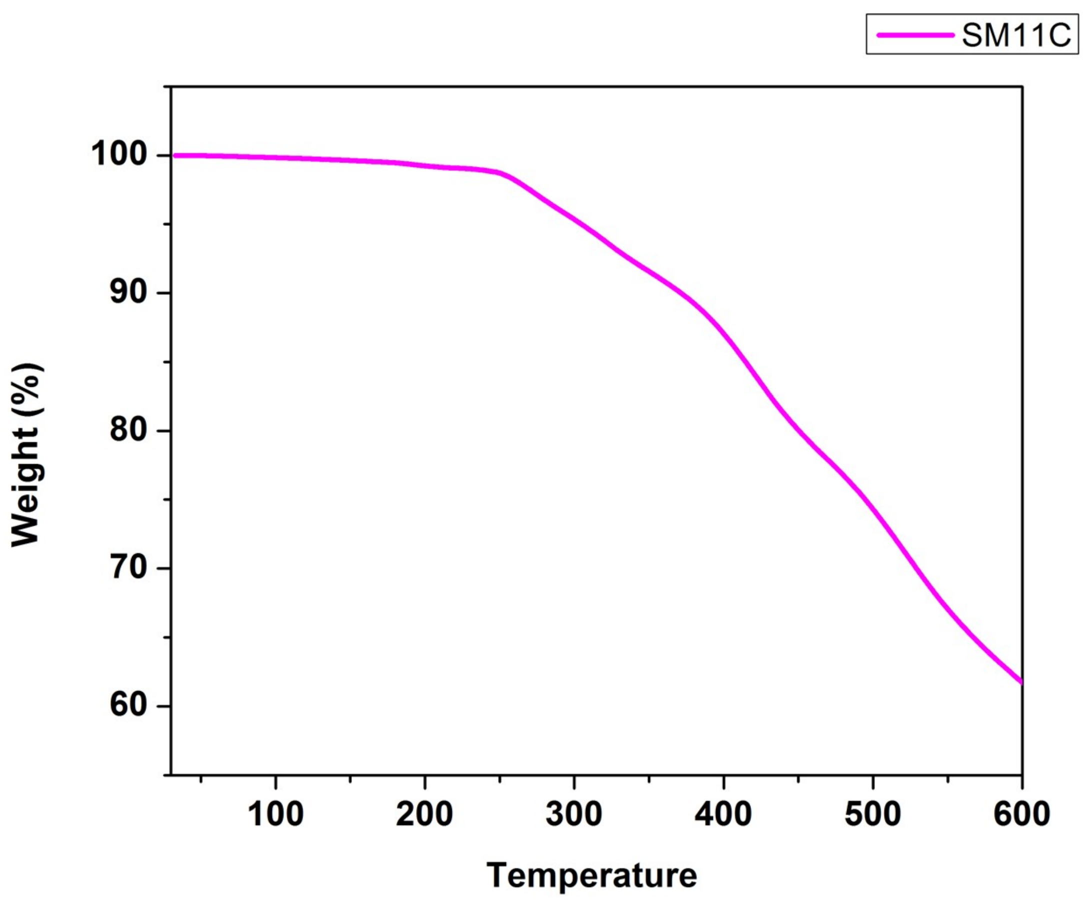

Fig. S11 Thermo Gravimetric Analysis of CP **2** under nitrogen atmosphere showing stability of complex is very appreciable up to 250ºC.

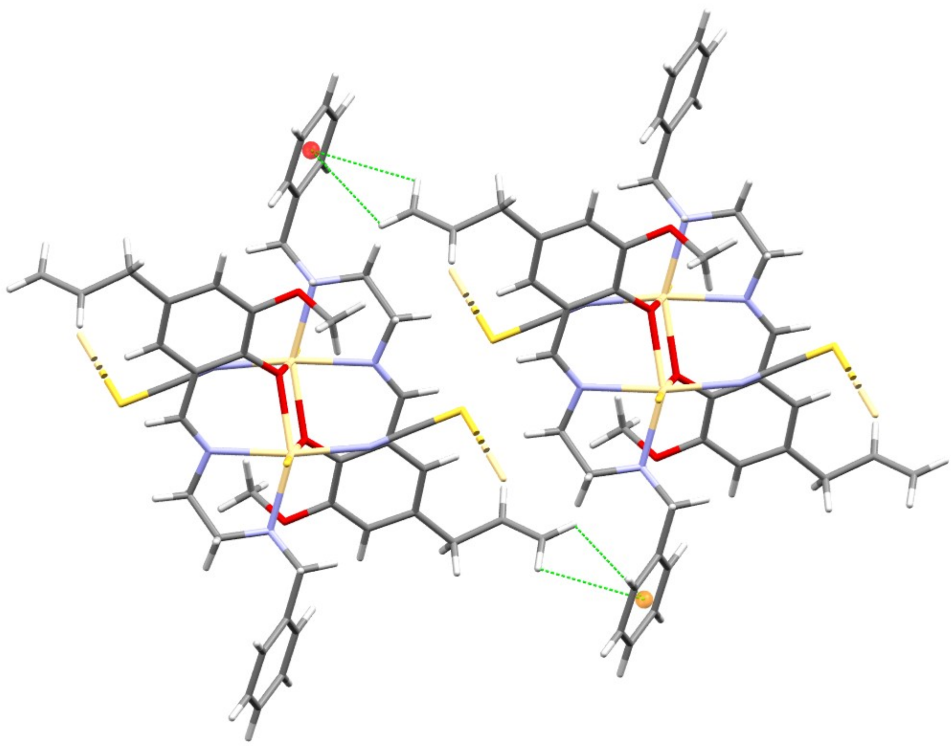

Fig. S12 Intermolecular C-H⋯π interaction of CP **1**

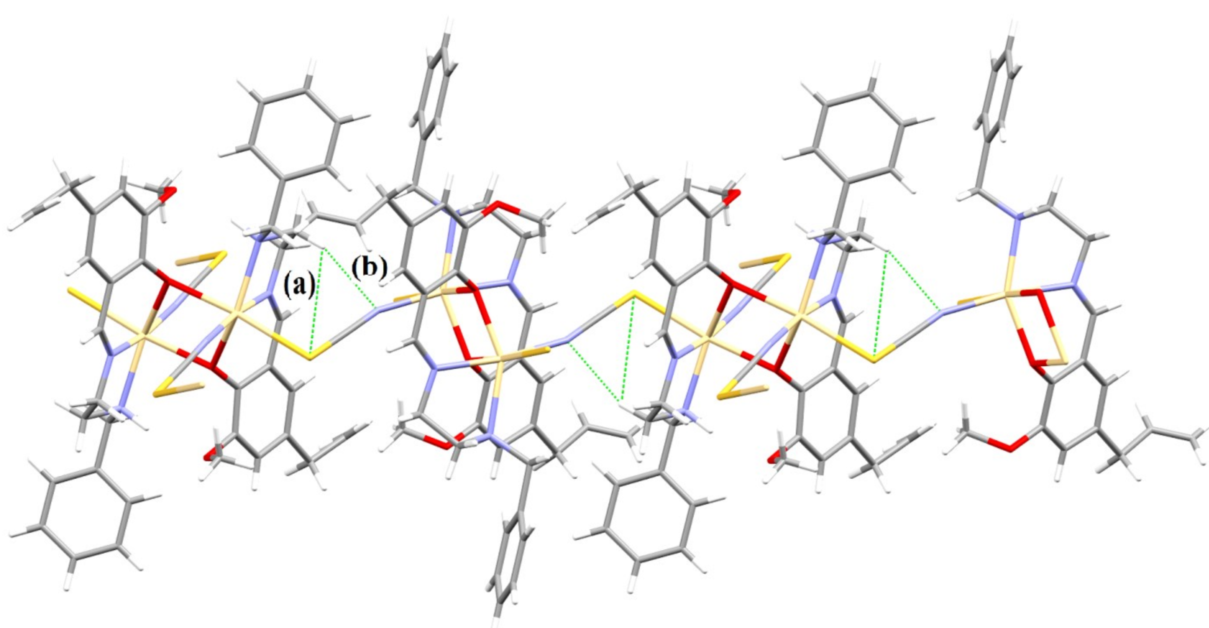

Fig. S13 Intramolecular **(a)** C-H⋯S (3.319 Å) and **(b)** C-H⋯N (2.563 Å) interaction of CP **1**

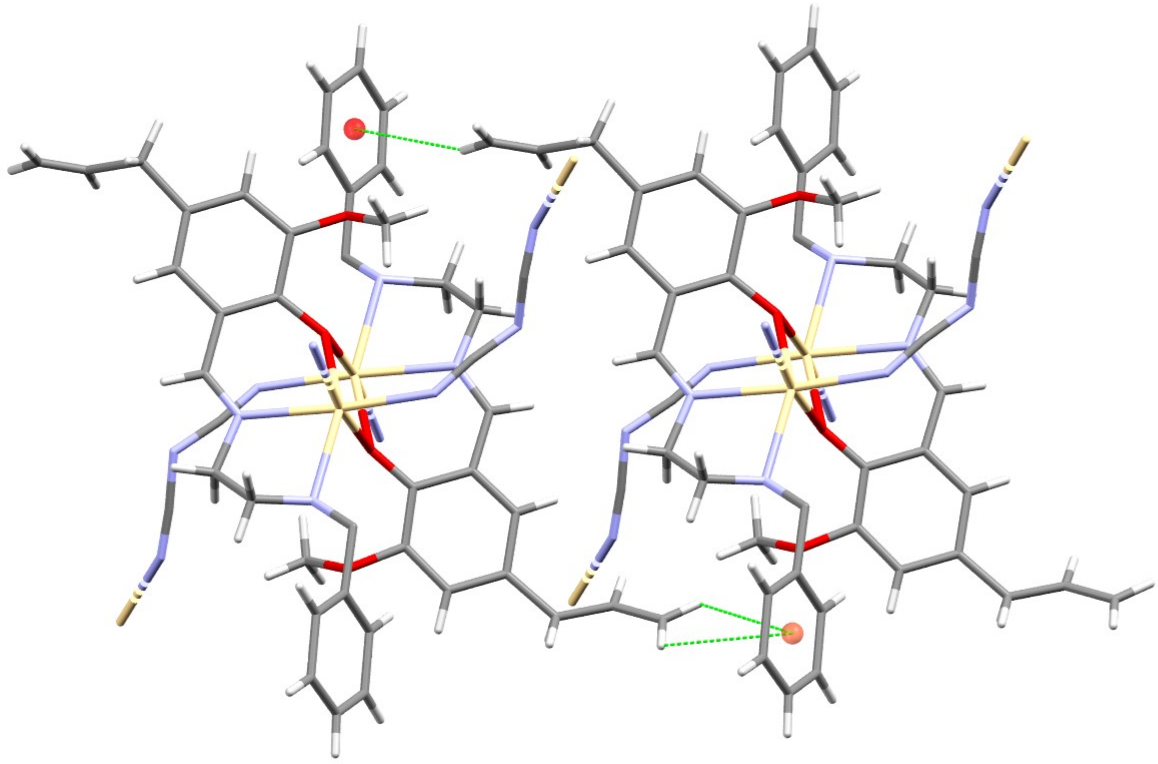

Fig. S14 Intermolecular C-H···π interaction of CP **2**

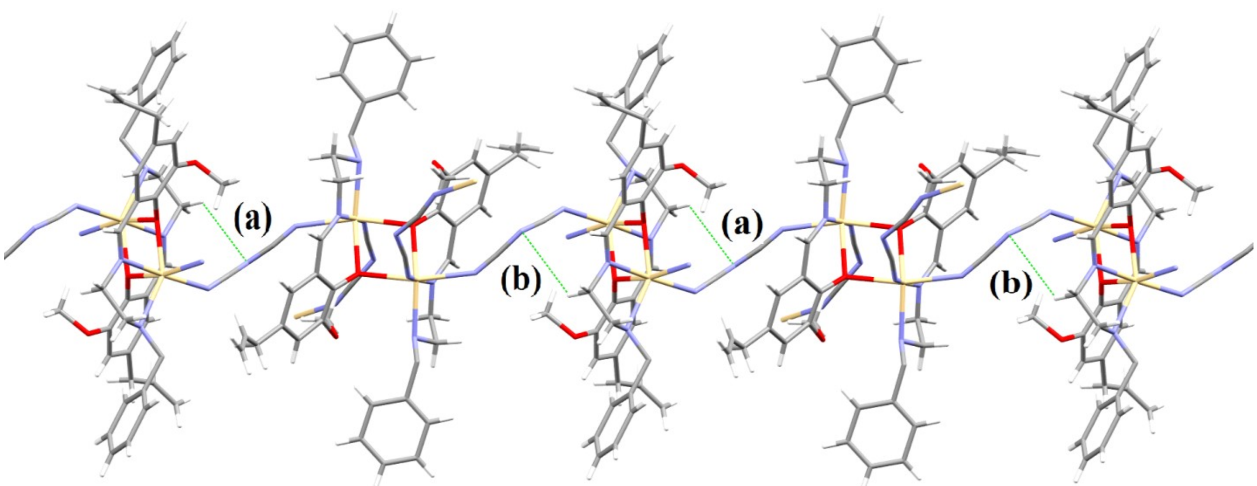

Fig. S15 Intramolecular **(a) C-H···N** (3.305 Å) and **(b) C-H···N** (3.178 Å) interaction of CP **2**

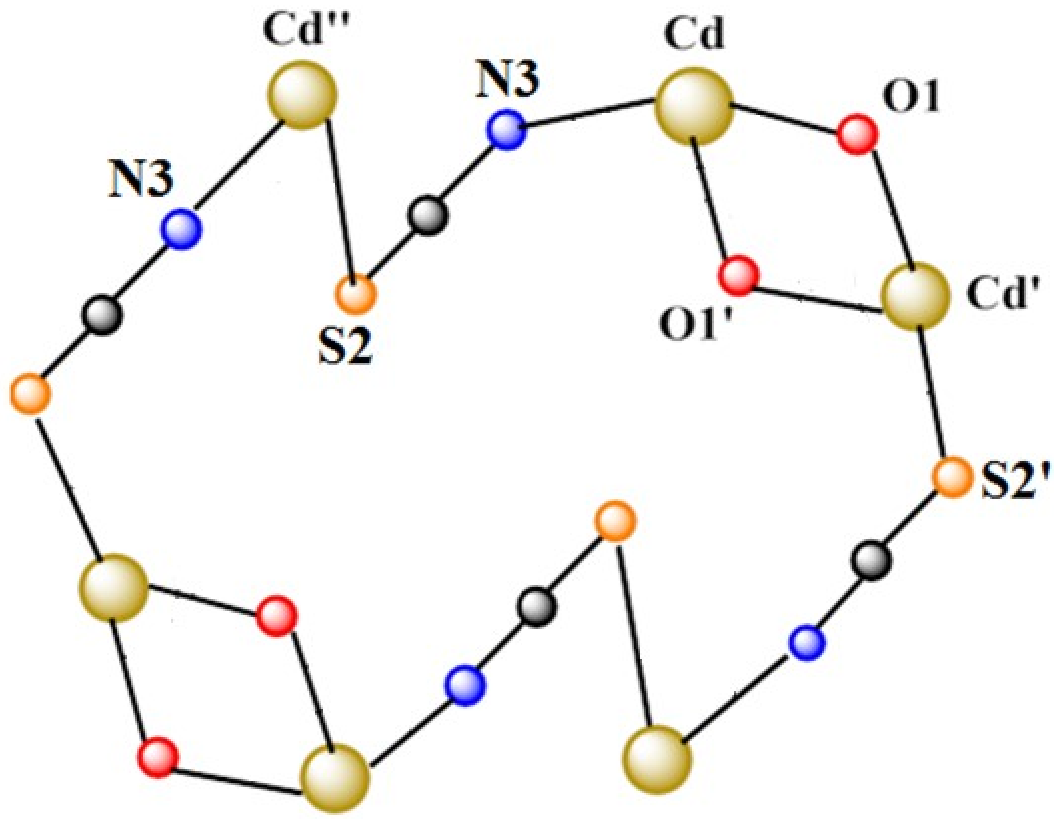

Fig. S16. The repeating cage of the polymeric chain of CP**1.** (Symmetry code: Cd **':** *x*, 1.5-*y*, 1/2 +*z*; S2**':** 1-*x*, 1/2+*y*, 1.5-*z*; O1': *x*, 1.5-*y*, 1/2+*z*; Cd **'':** 1-*x*, 1-*y*, 1-*z*; N3**:** 1-*x*, 2-*y*, 1-*z*).

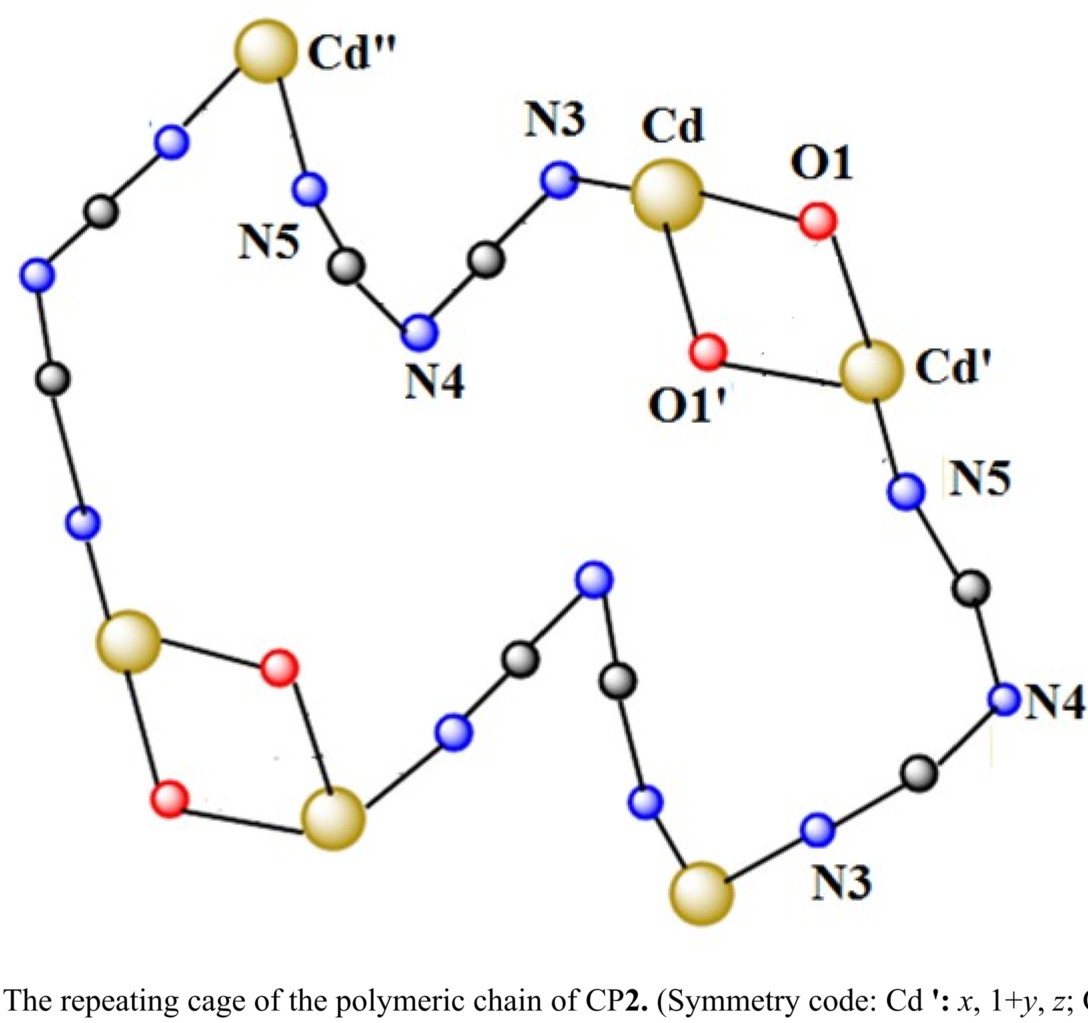

Fig. S17. The repeating cage of the polymeric chain of CP**2.** (Symmetry code: Cd **':** *x*, 1+*y*, *z*; O1**'**: *x*, 1+*y*, *z*; Cd **'':** 1/2+*x*, 1-*y*, 1/2+*z*; N5: 1/2+*x*, 1-*y*, 1/2+*z*).

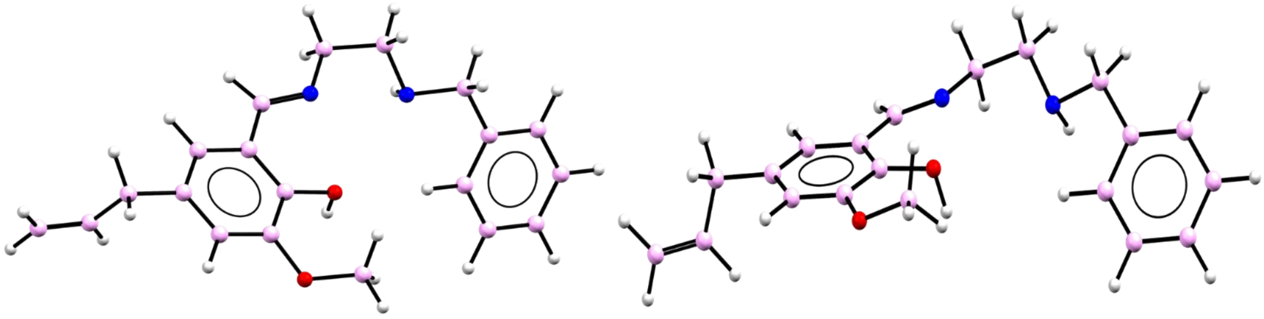

Fig. S18. The non-planar nature of the ligand **HL**

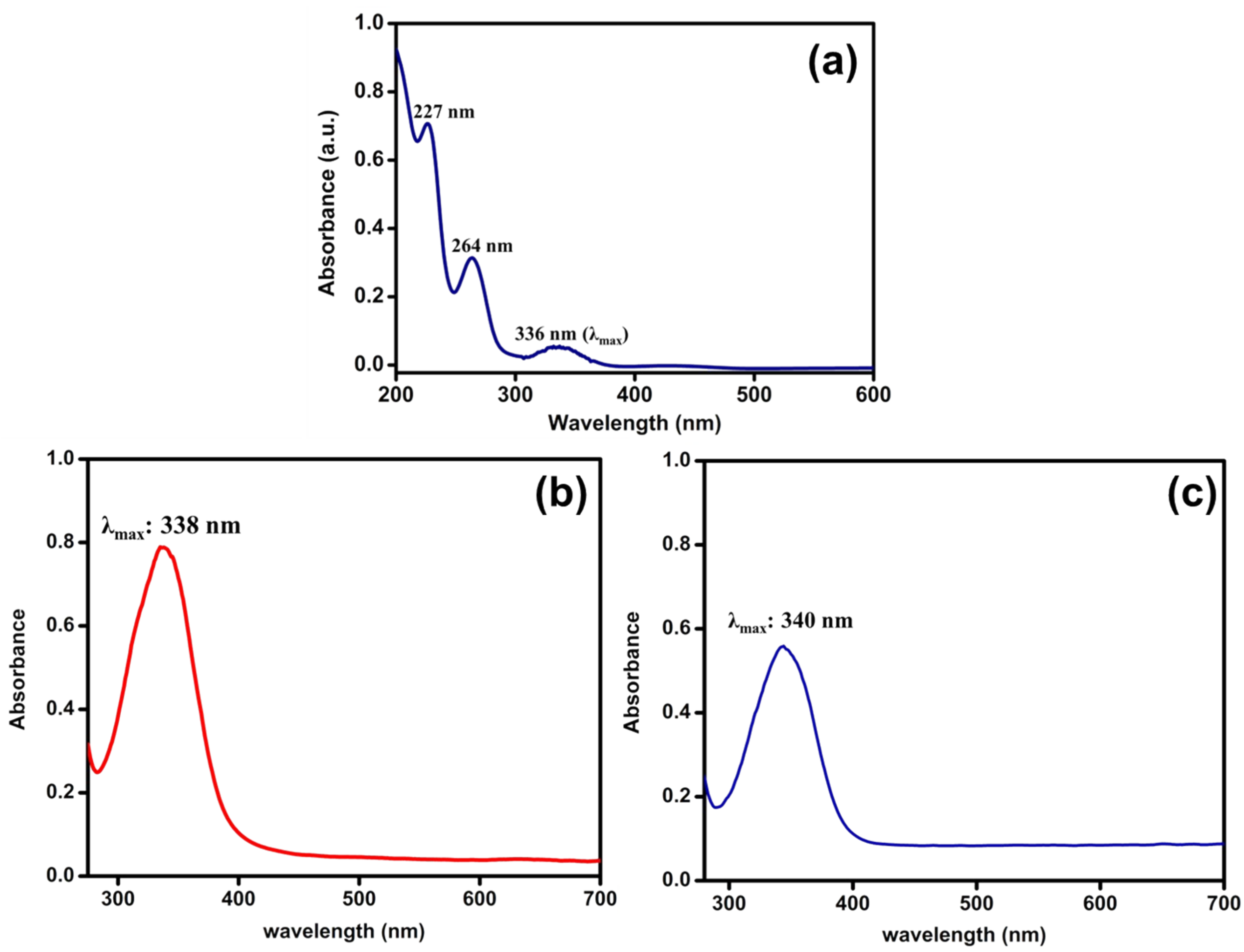

Fig. S19 UV-Vis absorption spectra of ligand HL (a), and acetonitrile dispersion of CP **1** (b) and **2** (c).

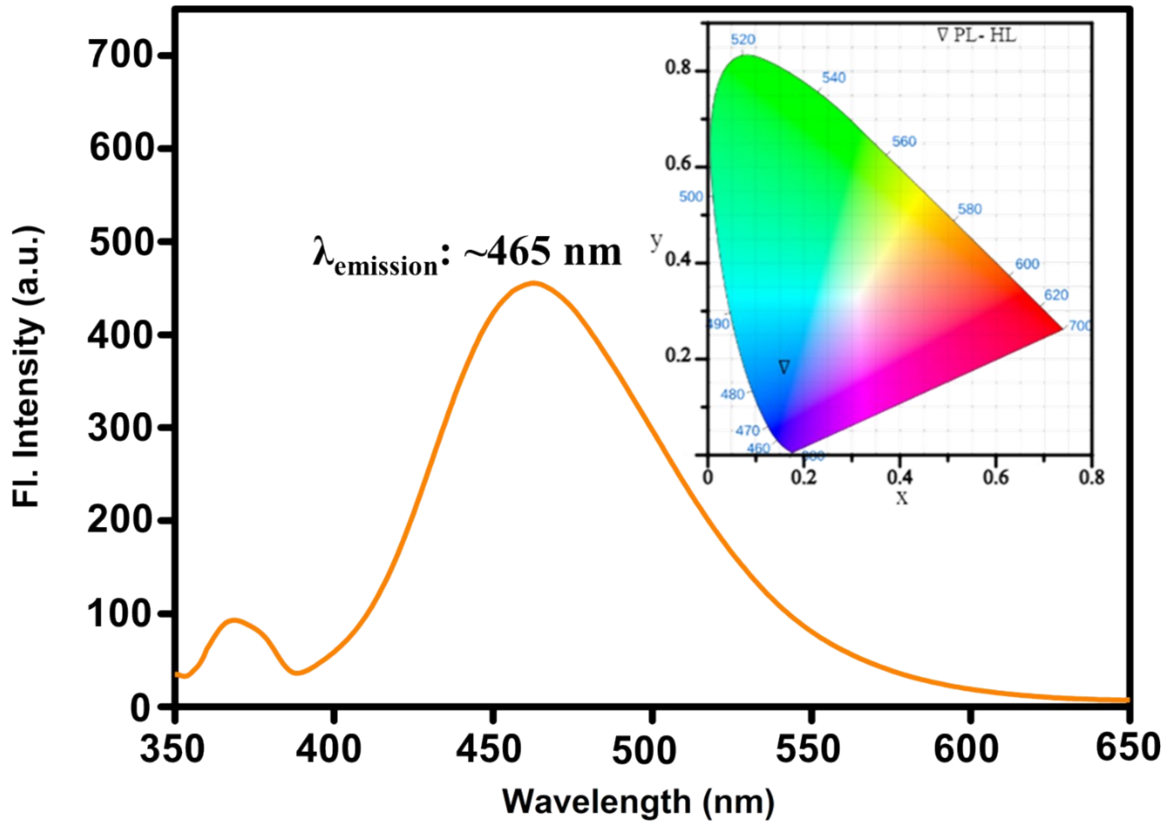

Fig. S20 Emission profile of HL [inset: CIE 1931 chromaticity diagram]

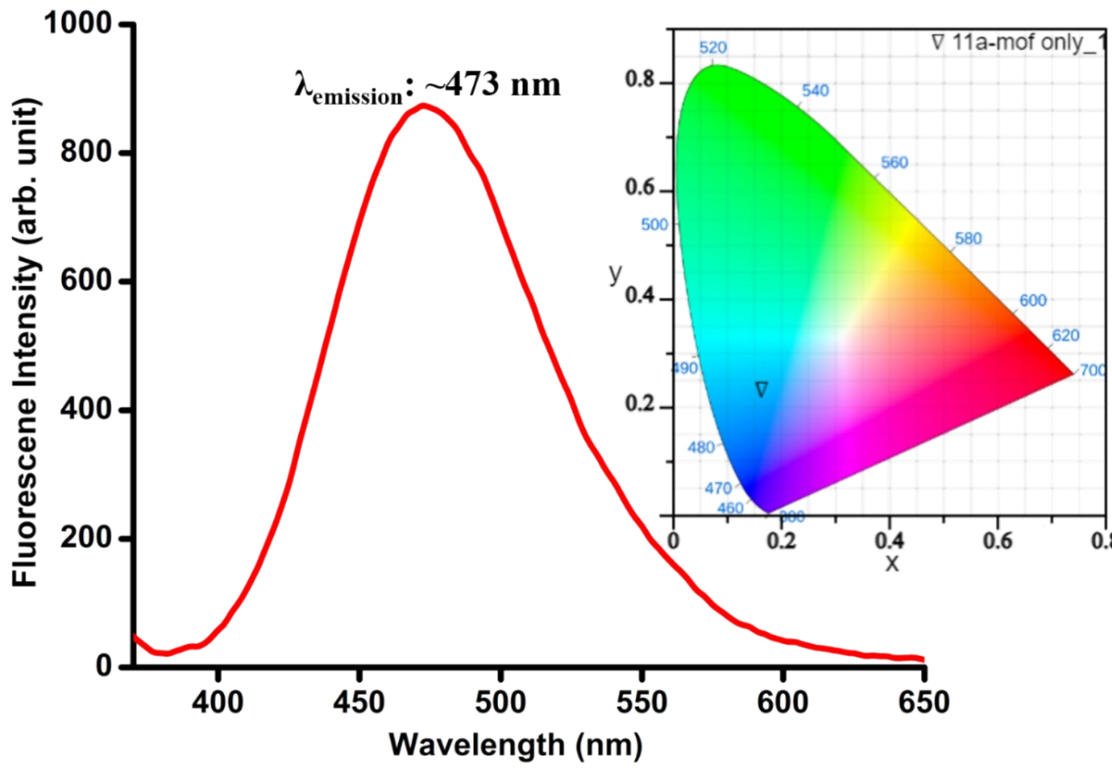

Fig. S21 Emission profile of CP **1** (dispersed in acetonitrile, $\lambda_{excitation}$: 340 nm) and CIE 1931 chromaticity diagram depicting its blue fluorescence.

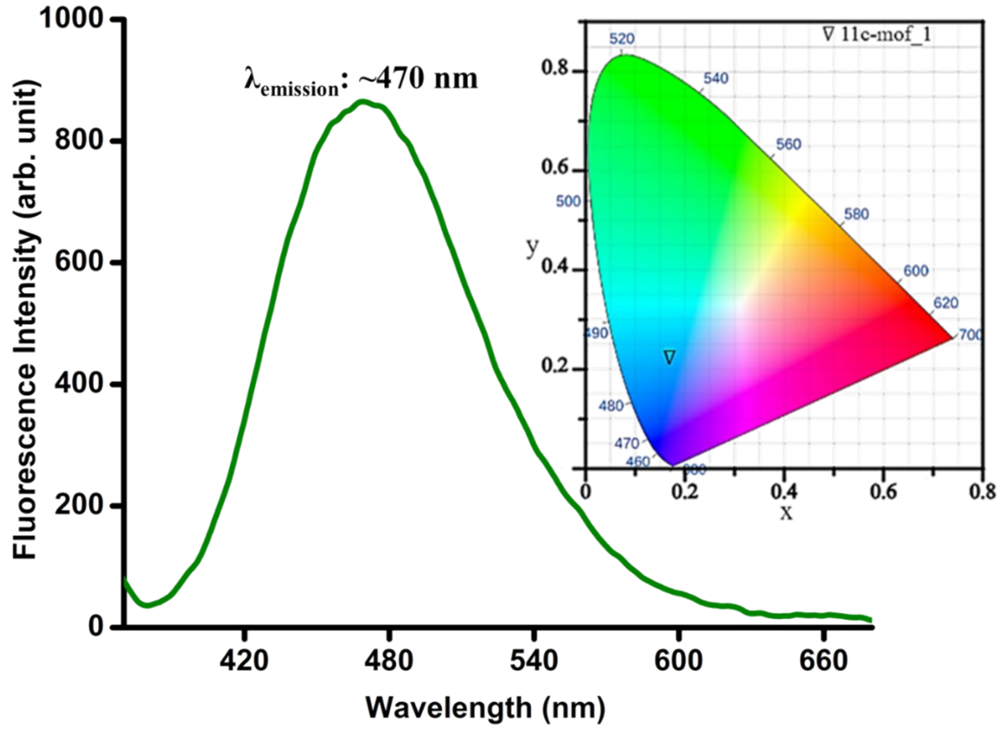

Fig. S22 Emission profile of CP **2** (dispersed in acetonitrile, $\lambda_{excitation}$: 340 nm) and CIE 1931 chromaticity diagram depicting its blue fluorescence.

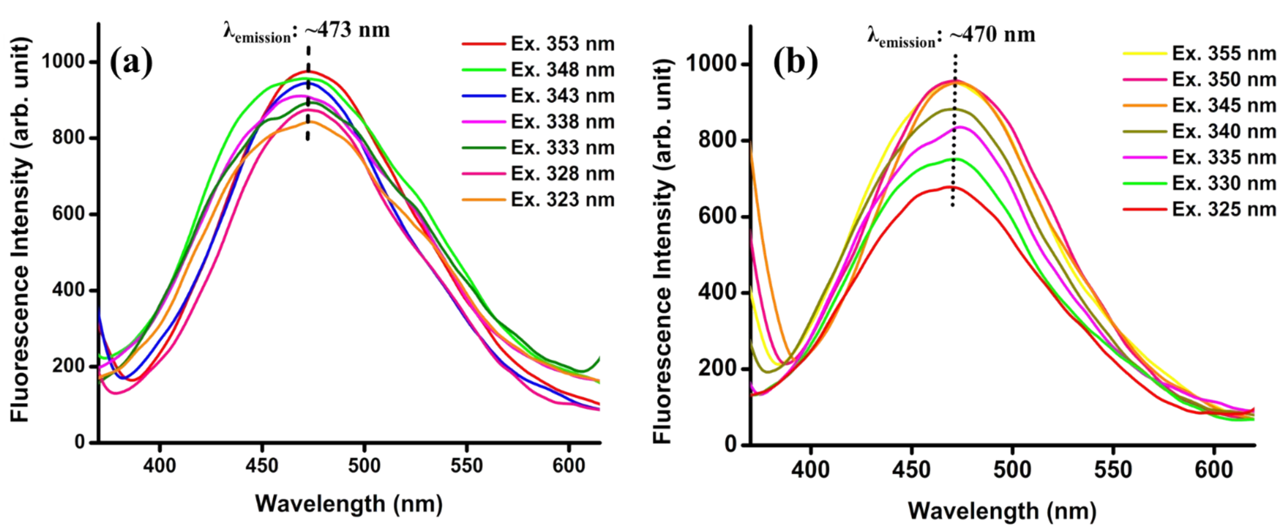

Fig. S23 Excitation dependent fluorescence profile of CP **1** and **2** : determination of true emission peak.

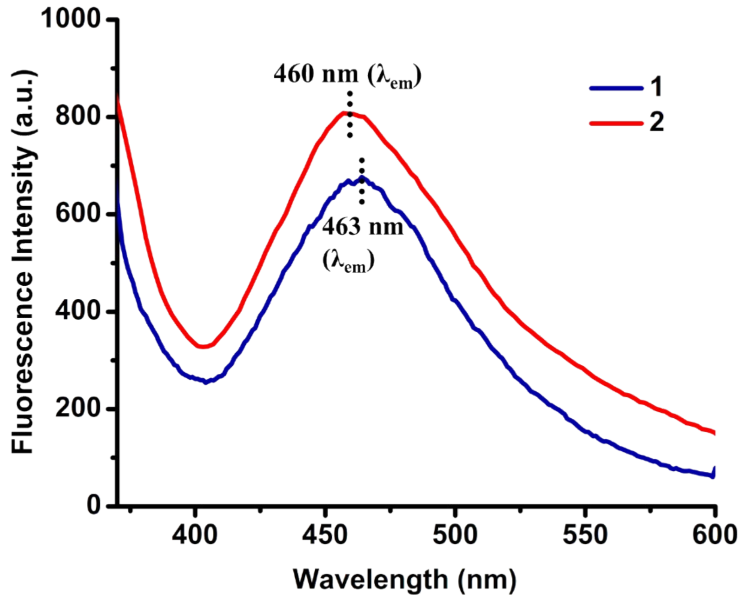

Fig. S24 Solid phase emission profile of powdered CP **1** and **2**.

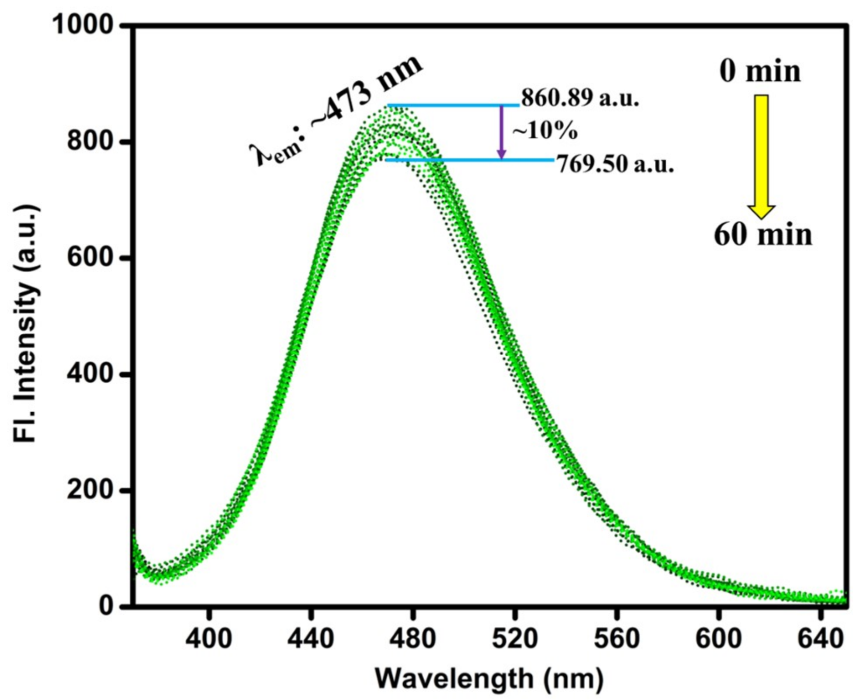

Fig. S25 Inspection of appropriate homogenization and photostability of the CP **1** - acetonitrile dispersion at continuous $\lambda_{excitation}$: 340 nm for a time period 0-60 minutes.

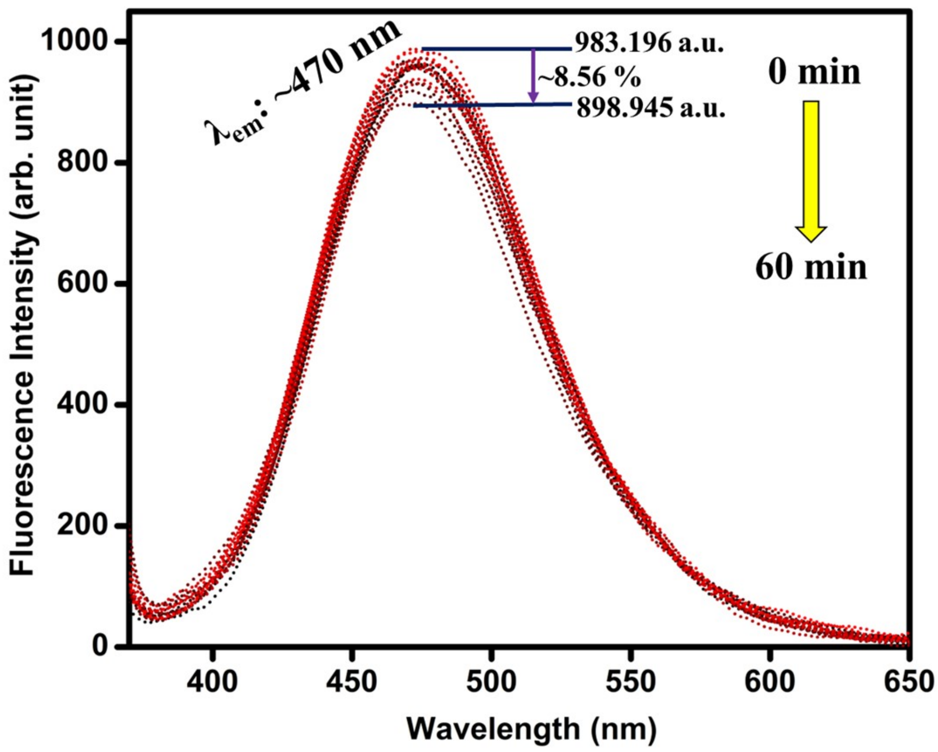

Fig. S26 Inspection of appropriate homogenization and photostability of the CP **2 -** acetonitrile dispersion at continuous $\lambda_{excitation}$: 340 nm for a time period of 0-60 minutes.

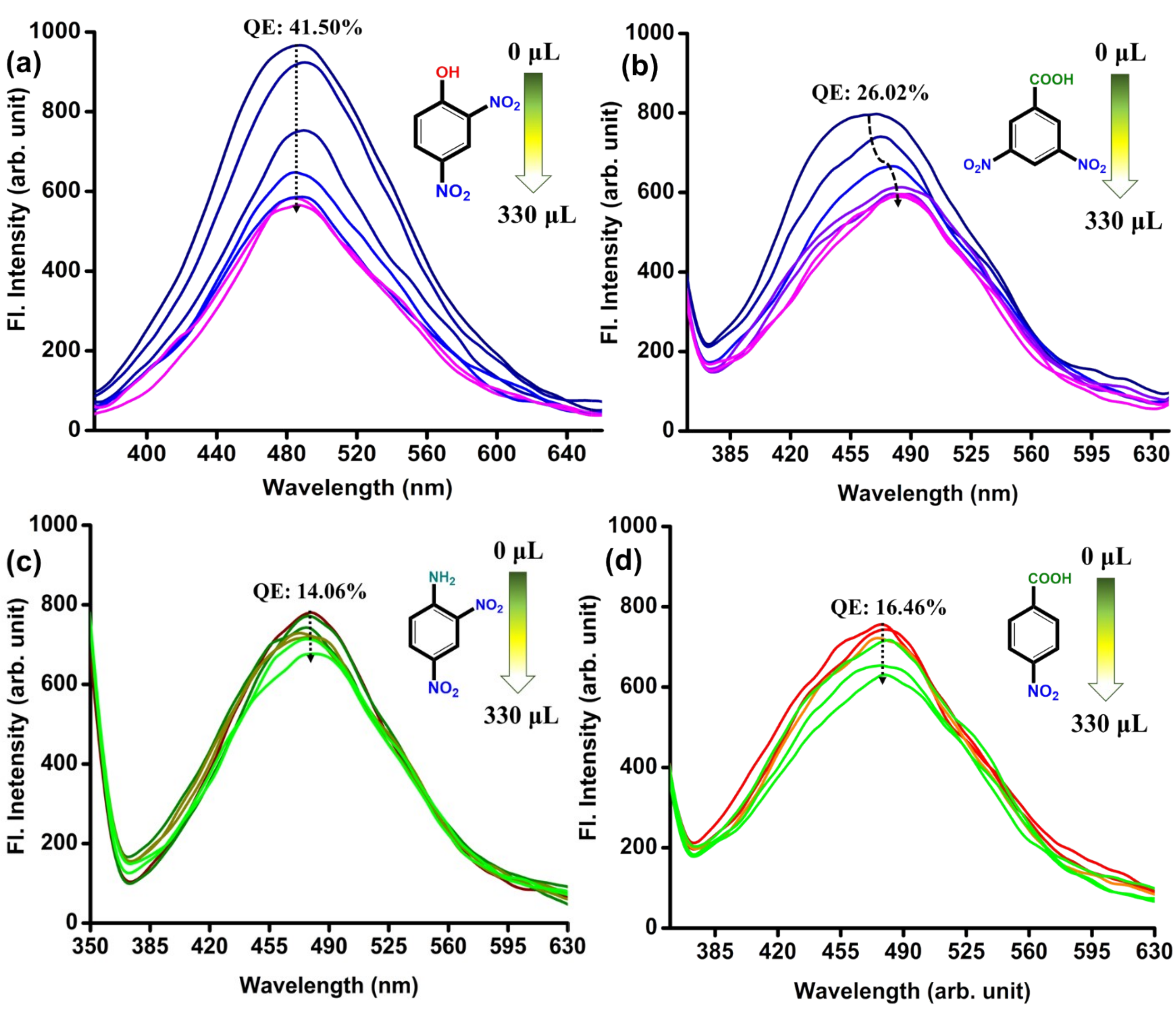

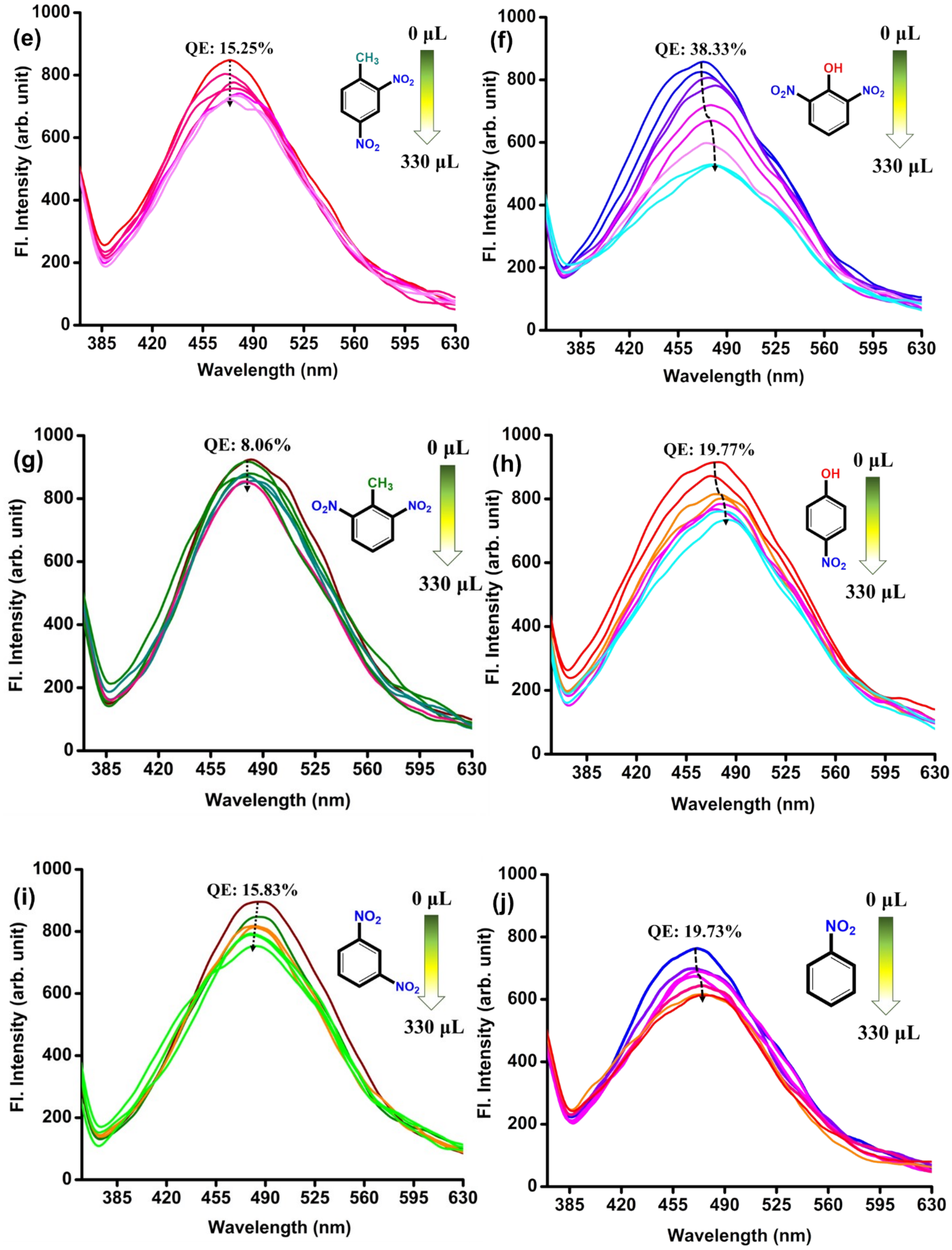

Fig. S27. Emission profile of **1**-acetonitrile dispersion upon gradual addition of 10^{-4} M aq. solution of other nitro-analytes (NACs): (a) 2,4-DNP, (b) DNBA, (c) DNA, (d) NBA, (e) DNT, (f) 2,6-DNP, (g) 2,6-DNT, (h) NP, (i) DNB, (j) NB.

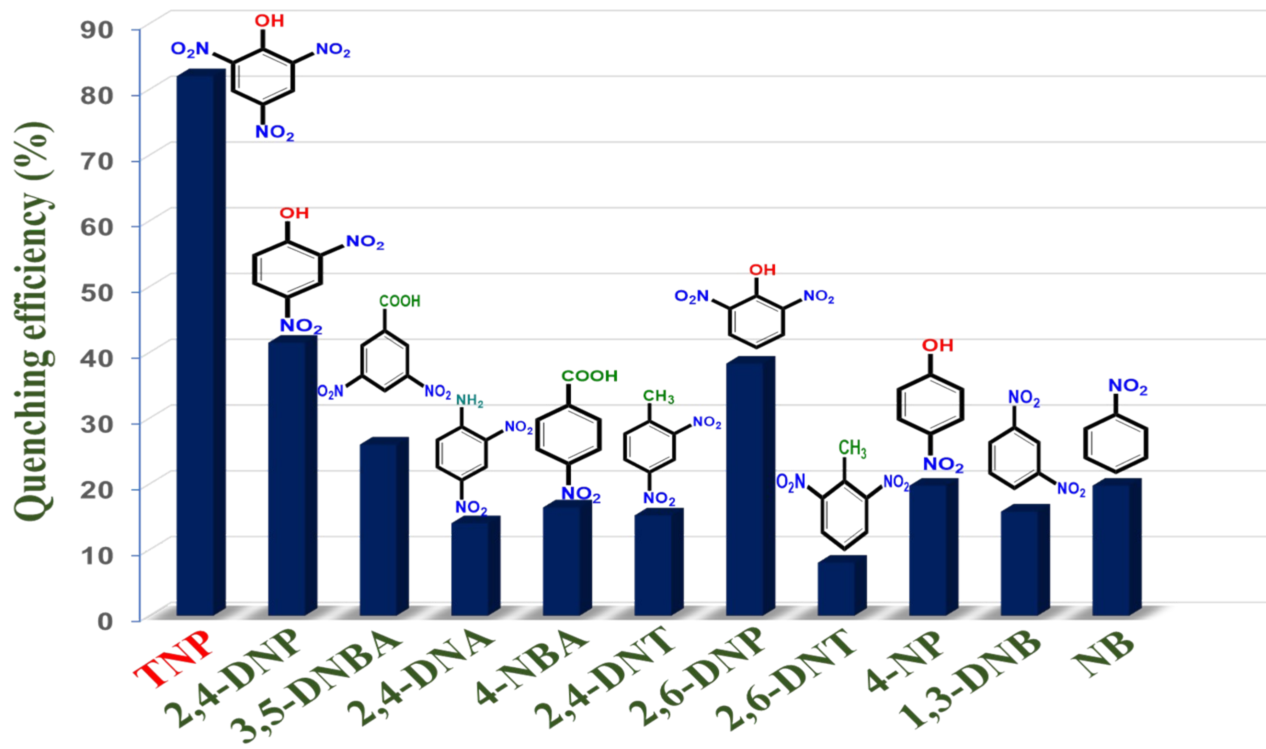

Fig. S28 Bar chart showing the comparative quenching efficiency (QE) of the NAC series towards the luminescence profile of **1**

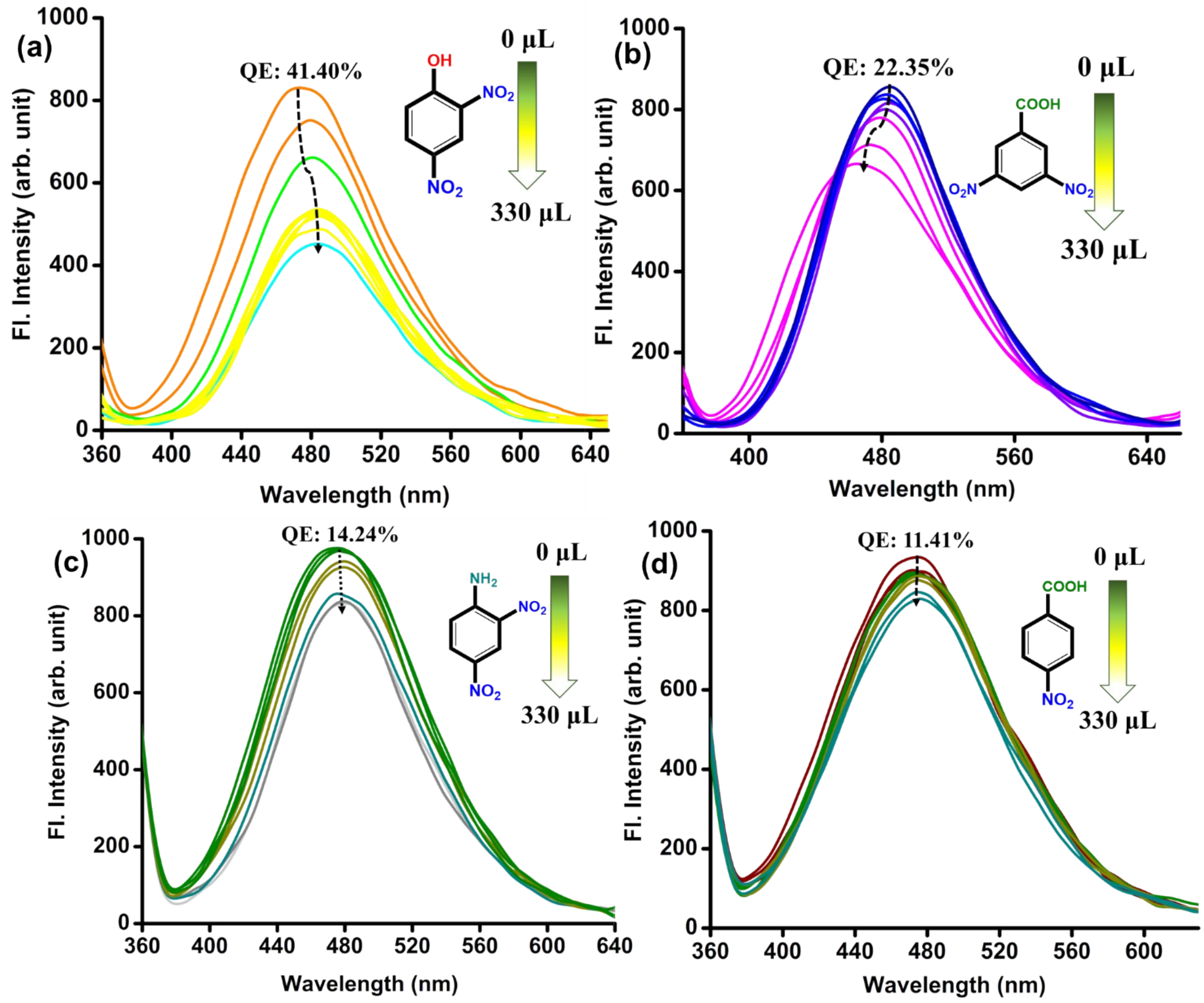

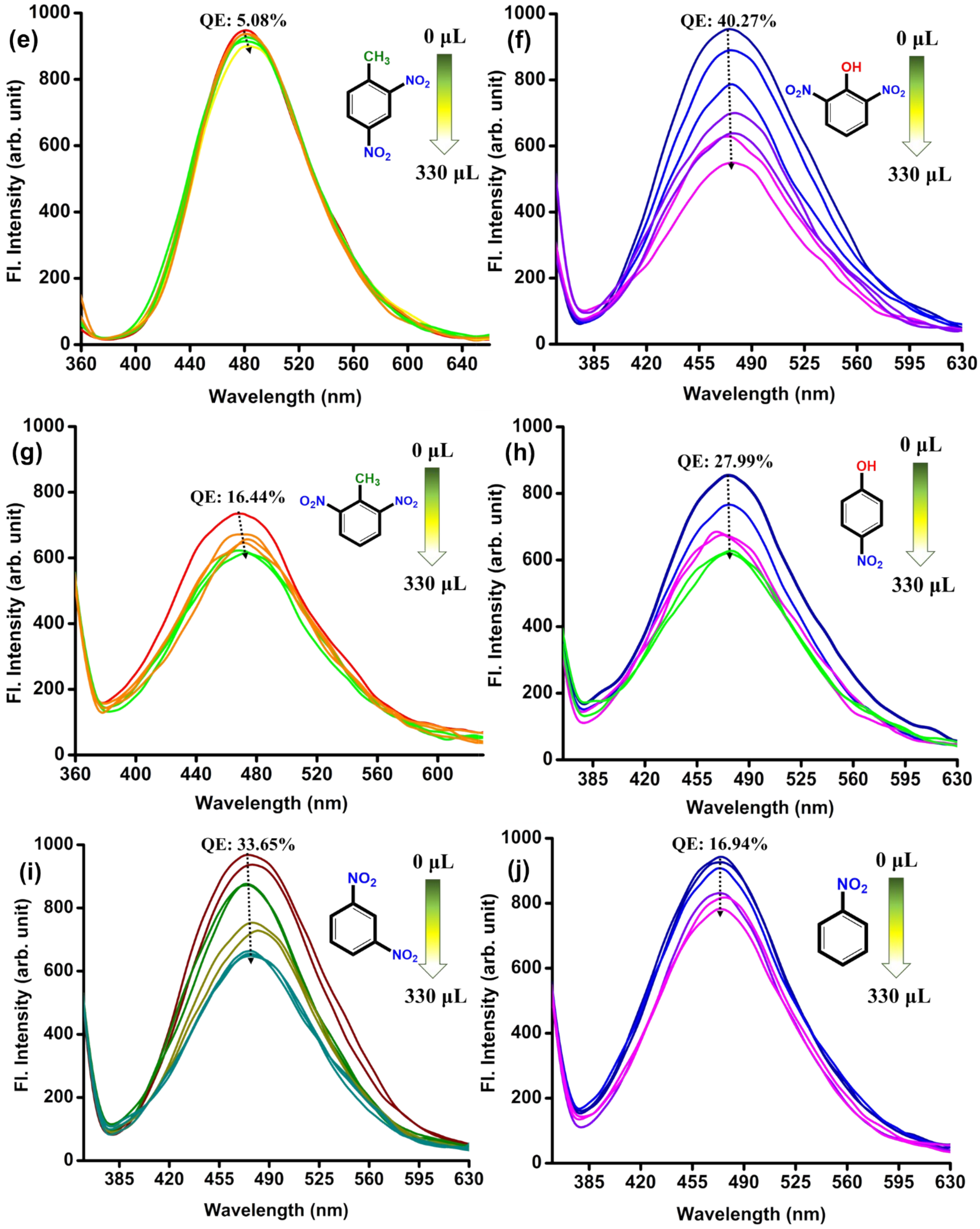

Fig. S29 Emission profile of CP **2**-acetonitrile dispersion upon gradual addition of 10^{-4} M aq. solution of other nitro-analytes: (a) 2,4-DNP, (b) DNBA, (c) DNA, (d) NBA, (e) 2,4-DNT, (f) 2,6-DNP, (g) 2,6-DNT, (h) NP, (i) DNB, (j) NB

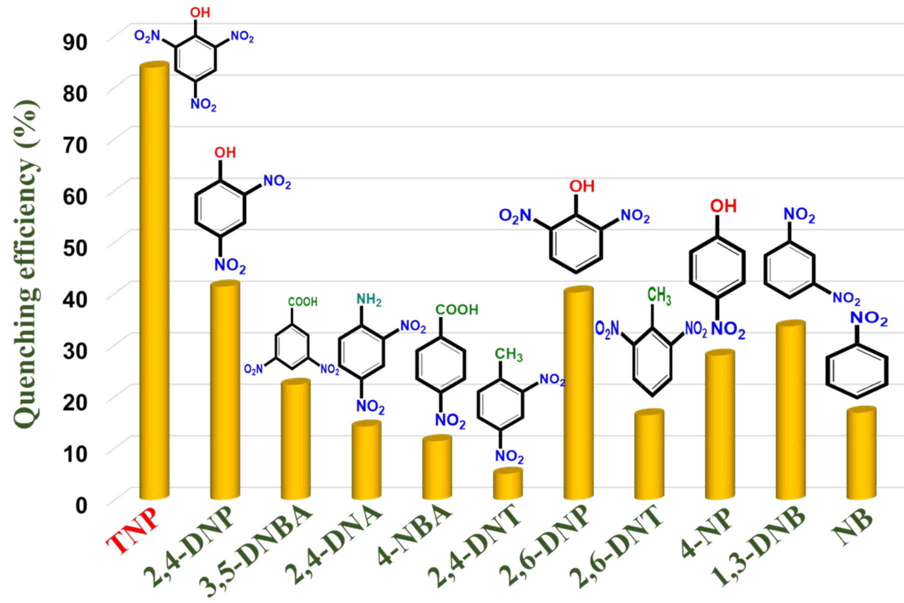

Fig. S30 Bar chart showing the comparative quenching efficiency (*QE*) of the NAC series towards the luminescence profile of **2.**

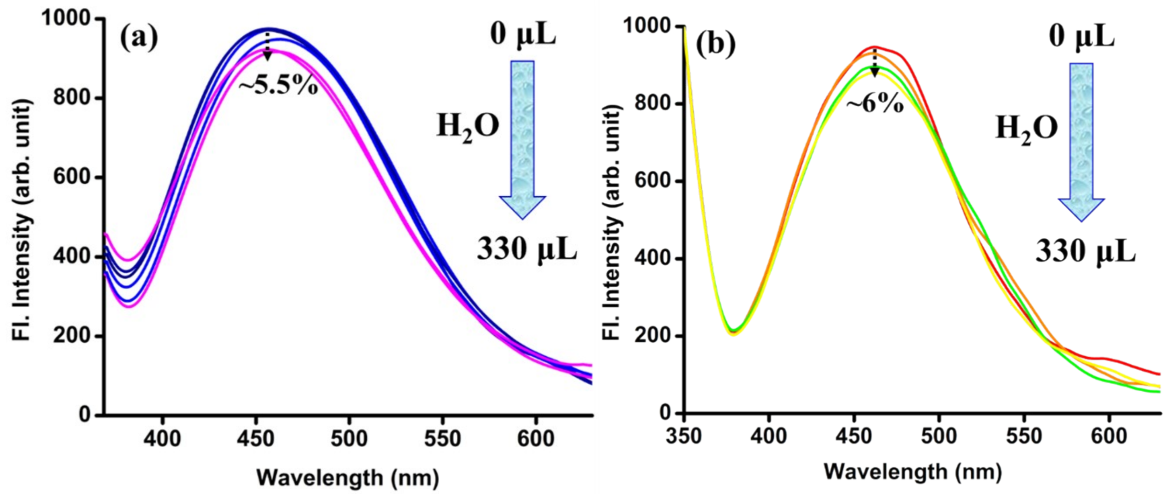

Fig. S31 Effect of addition of water (detection medium) on the emission profile of **1** and **2**

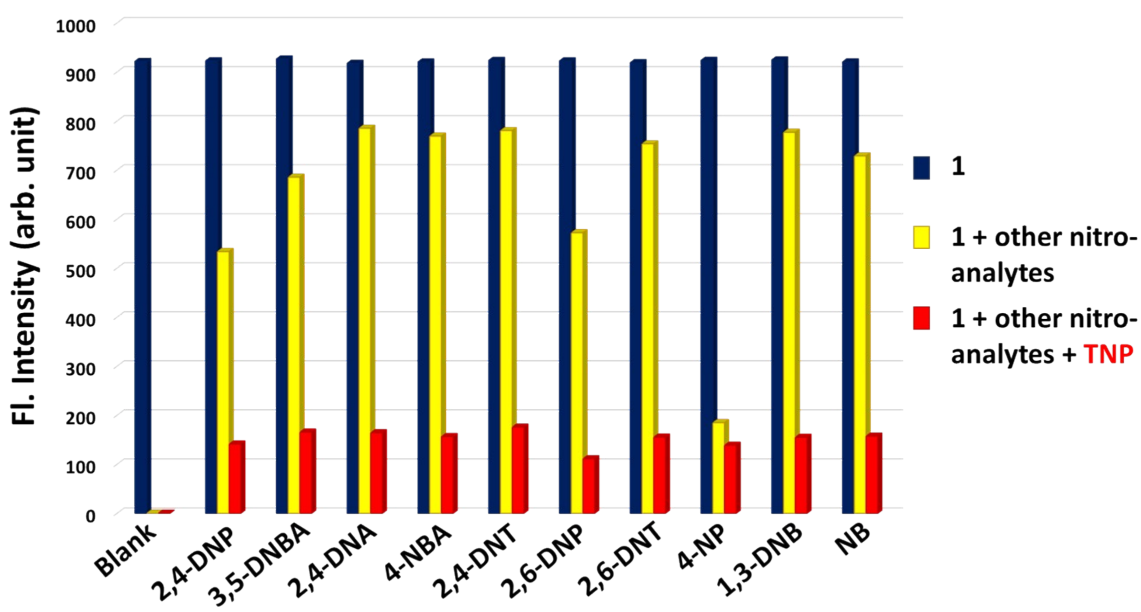

Fig. S32 Detection in a competitive environment: Competitive Analyte Test (CAT) for CP **1**, depicting high selectivity of the probe towards TNP.

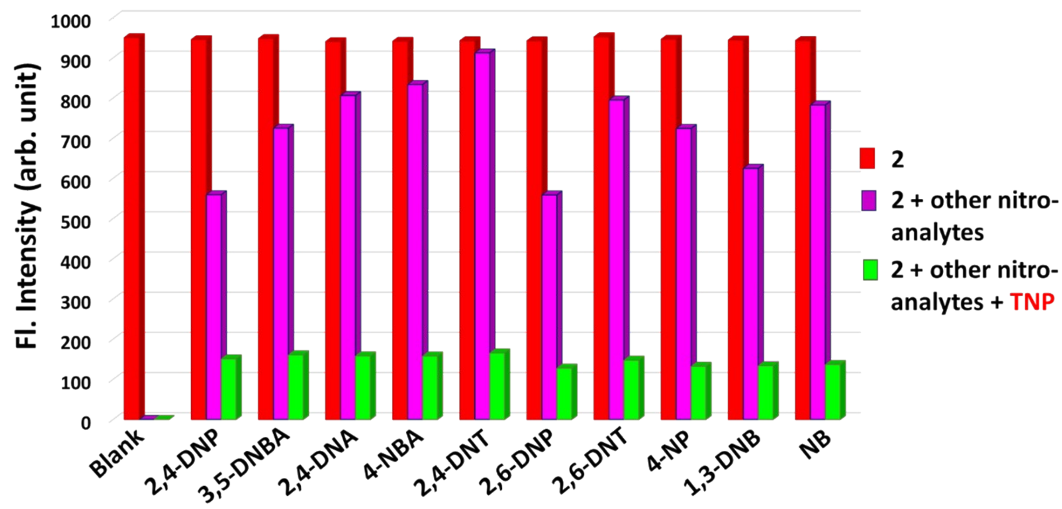

Fig. S33 Competitive analyte test (CAT) for CP **2,** affirming exclusive selectivity towards TNP.

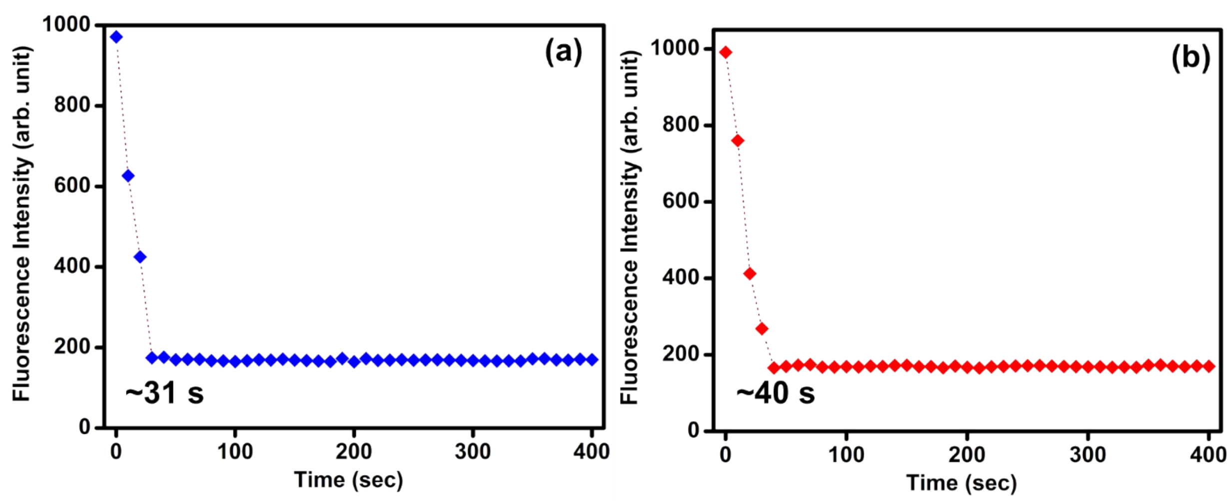

Fig. S34 Fast Responsive Analyte (FRA) test: estimation of response time of analyte interaction to the sensors: **1** (a) and **2** (b).

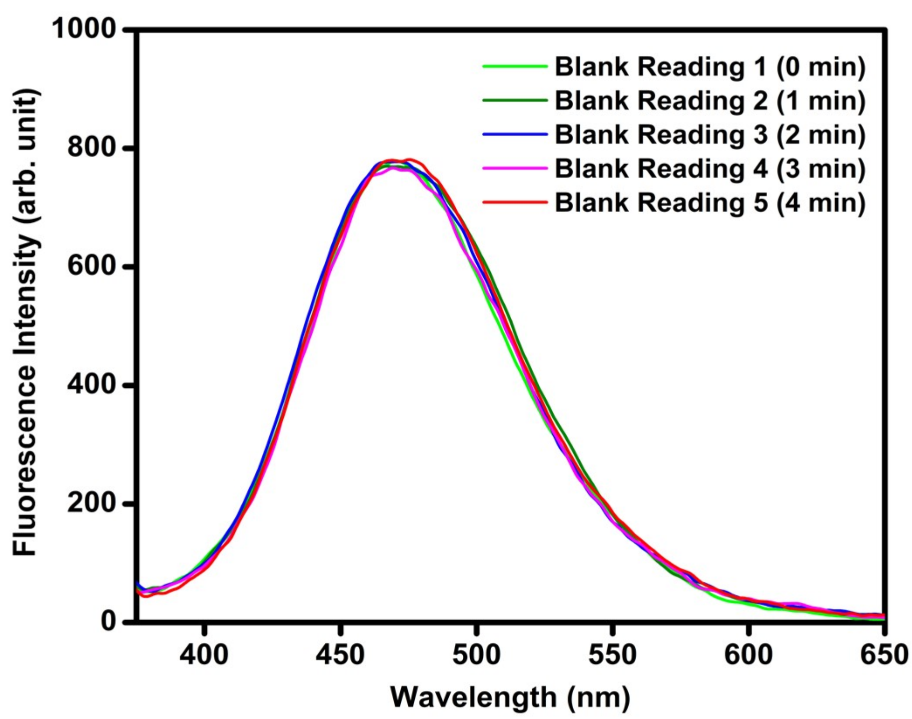

Fig. S35 Five consecutive Blank measurements of **1**/acetonitrile dispersion recorded at a regular interval of ~1 min**.**

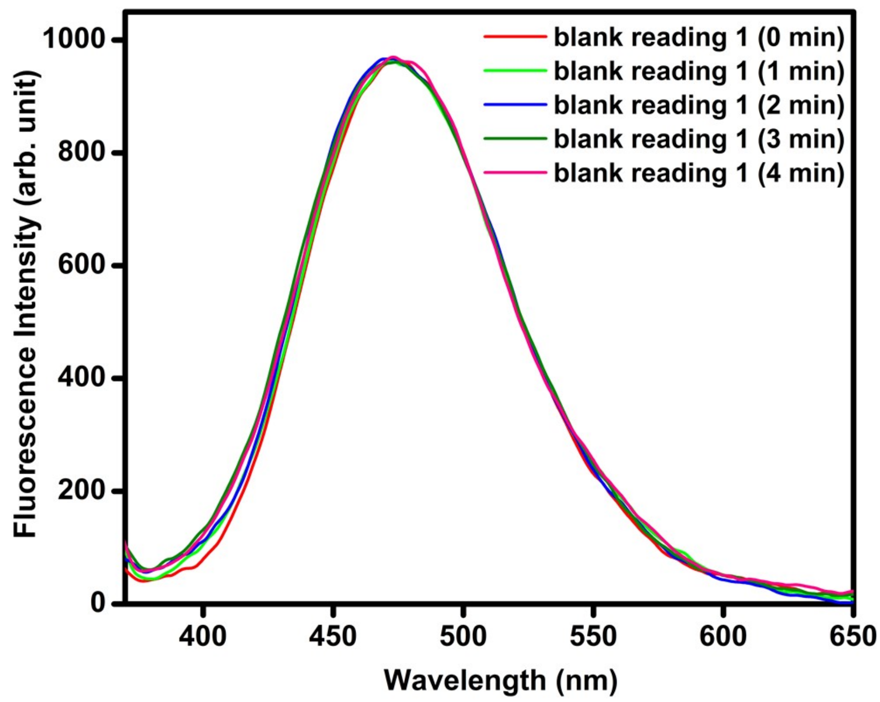

Fig. S36 Five consecutive Blank measurements of **2**/acetonitrile dispersion recorded at a regular interval of ~1 min**.**

Table S1 Calculation of Standard Deviation (σ):

CP **1**	
Blank Reading	**Fluorescence Intensity (a.u.)**
1	780.197
2	778.486
3	776.775
4	769.075
5	766.509
Value of σ	**6.049**
CP **2**	
Blank Reading	**Fluorescence Intensity (a.u.)**
1	970.024
2	966.654
3	962.895
4	962.247
5	960.822
Value of σ	**3.752**

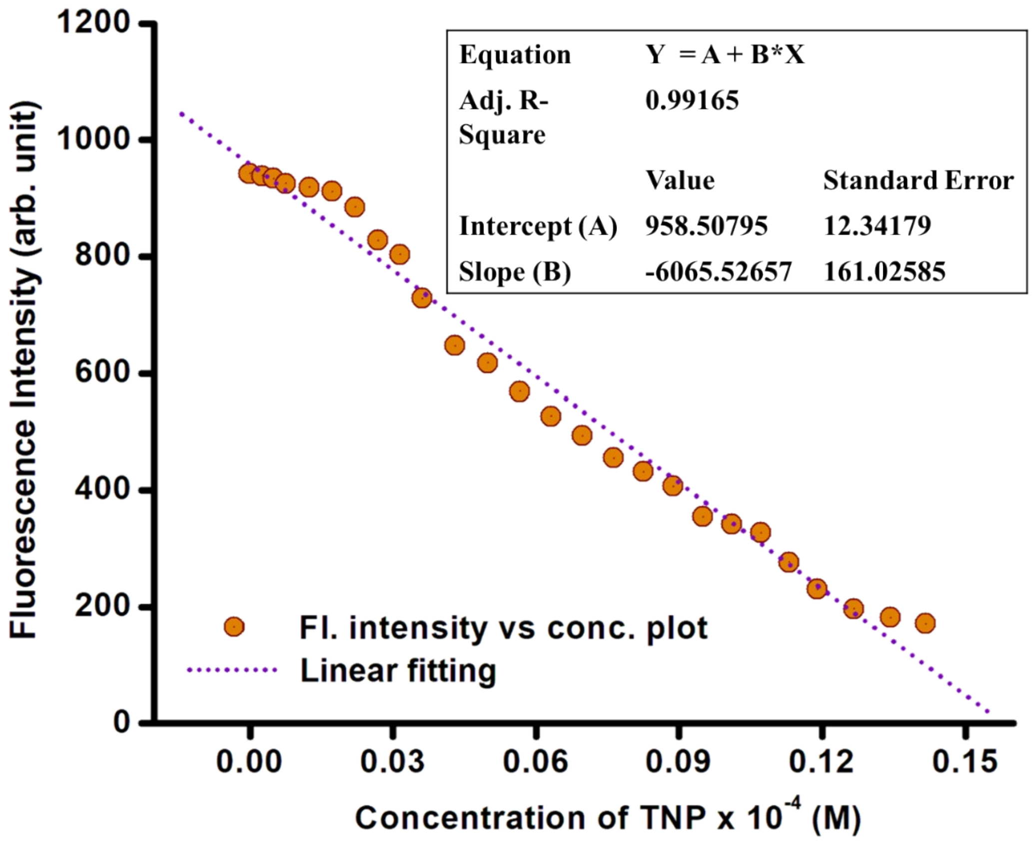

Fig. S37 Alteration in the PL intensity of **1** with increasing TNP concentration and corresponding linear fitting for evaluation of slope (k) used in $3\sigma/k$ equation.

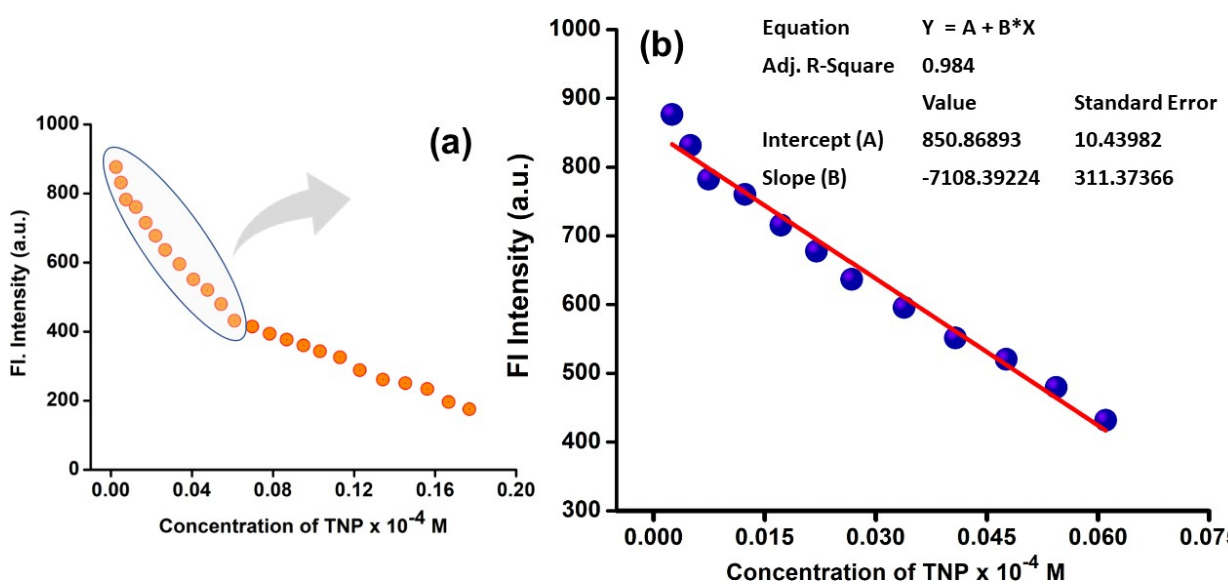

Fig. S38. (a) Alteration in the PL intensity of **2** with increasing TNP concentration: full range; **(b)** linear range of (a) for evaluation of slope (k) used in $3\sigma/k$ equation.

Table S2 Calculation of limit of detection (*LOD*)

1. *For CP **1***

   Std. deviation (σ) = 6.049

   Slope (k) = 6065.526

   Therefore, LOD ($3\sigma/k$) = 0.0029 for 10^{-4} M [TNP] *i.e.,*~**0.29 µM** for TNP.

2. *For CP **2***

   Std. deviation (σ) = 3.752

   Slope (k) = 7108.392

   Therefore, LOD ($3\sigma/k$) = 0.0015 for 10^{-4} M [TNP] *i.e.,*~**0.15 µM** for TNP.

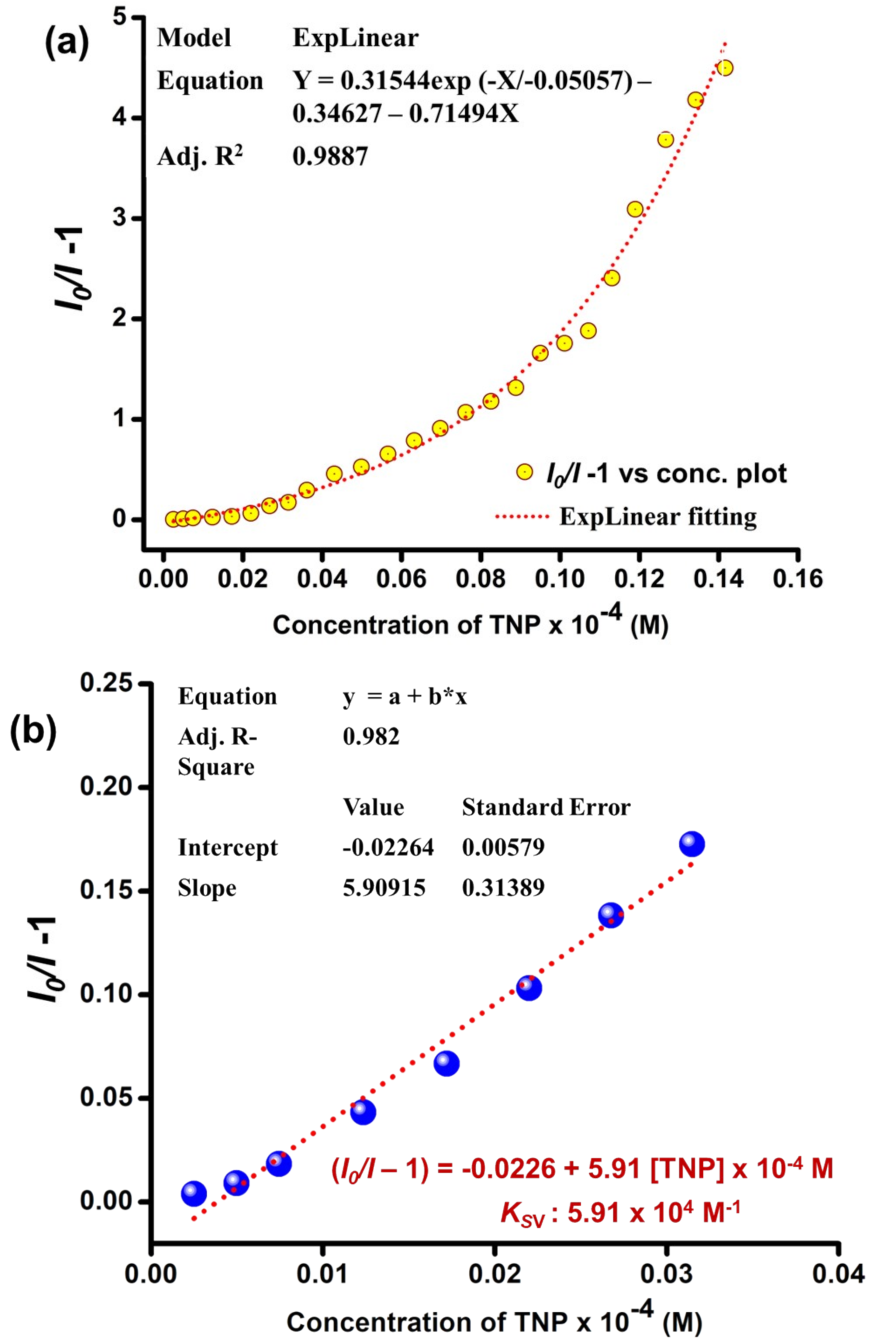

Fig. S39 **(a)** Full range of the Stern-Volmer (S-V) plot [$I_0/I - 1$ vs Concentration] of compound **1** with varying equivalent concentration of TNP along with its non-linear fitting; **(b)** linear range of the plot for calculation of quenching constant (K_{SV})**.**

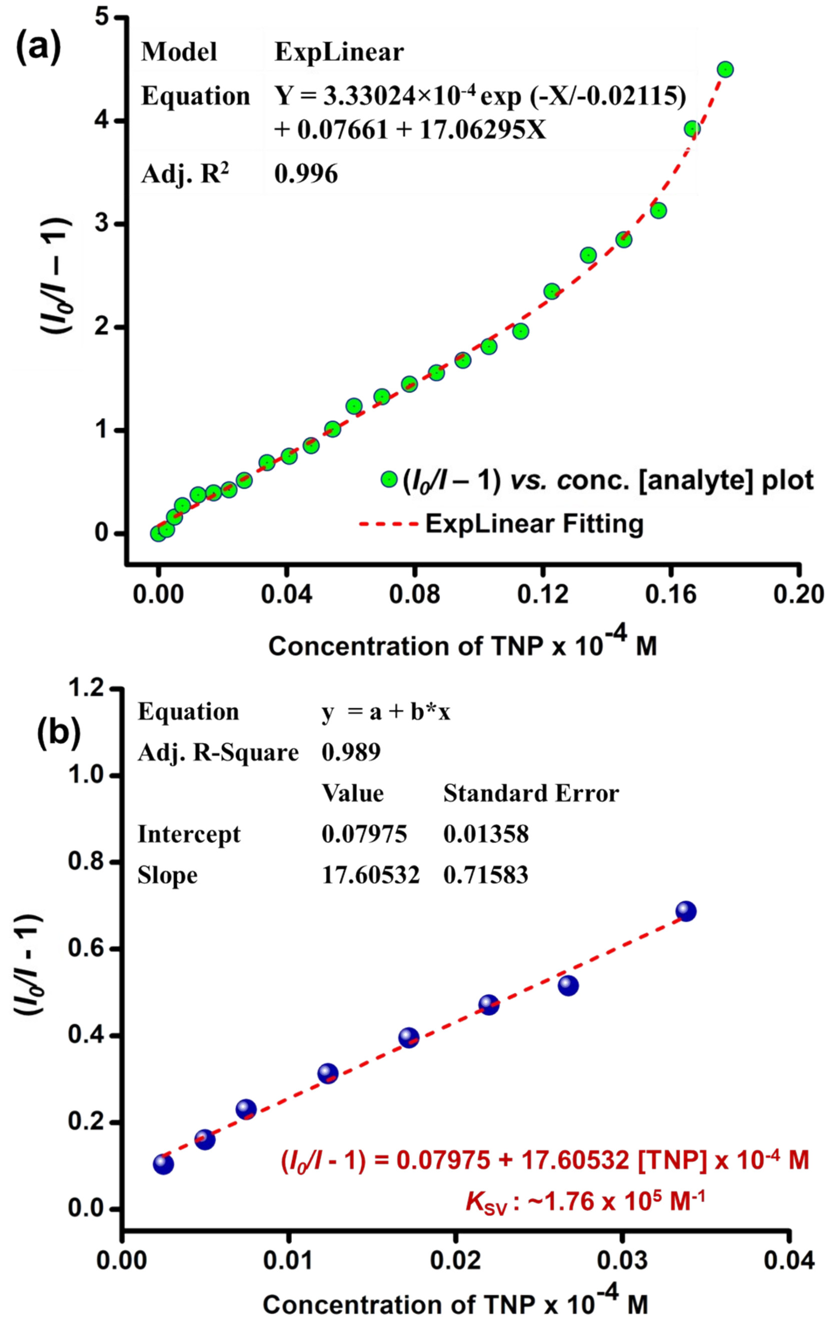

Fig. S40 (a) Full range of the Stern-Volmer (S-V) plot [$I_0/I - 1$ vs Concentration] of compound **2** with varying equivalent concentration of TNP along with its non-linear fitting; **(b)** linear range of the plot for calculation of quenching constant (K_{SV}).

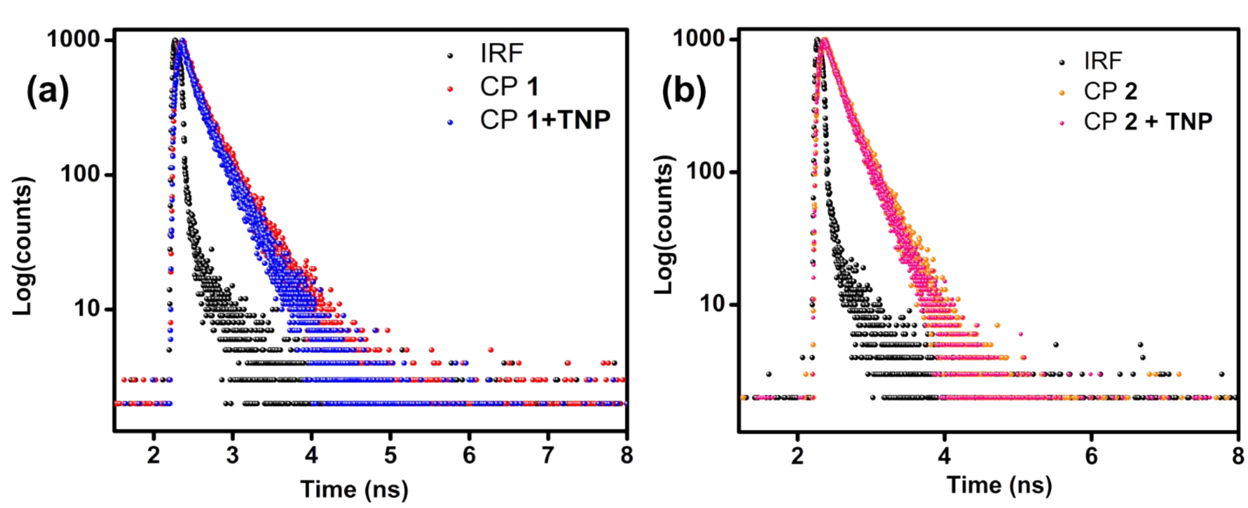

Fig. S41 Lifetime decay profile of **1** and **2** upon interaction with analyte TNP

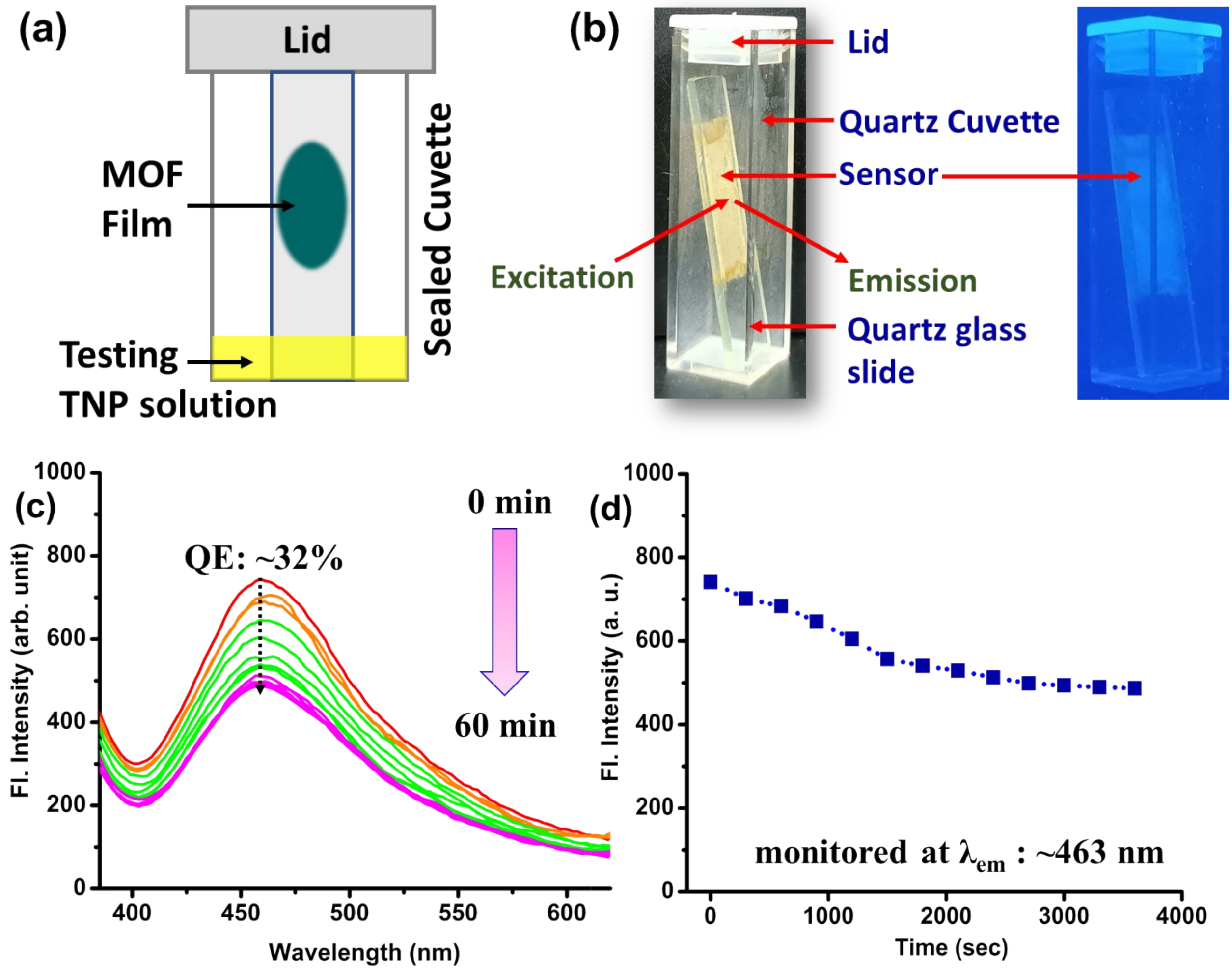

Fig. S42 (a) schematic representation and (b) physical image of the experimental set-up (under normal light and in UV-chamber) adapted for acetonitrile-mediated TNP vapour sensing study; (c) Fluorescence quenching (~32%) of **1** drop-casted on a quartz slide upon exposure of TNP (acetonitrile) vapour (up to ~60 minutes); (d) alteration of Fl. intensity as a function of elapsed time (monitored at ~463 nm).

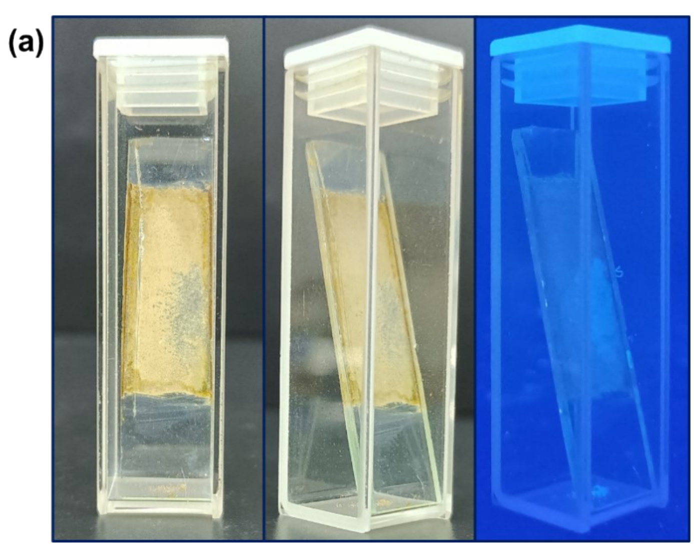

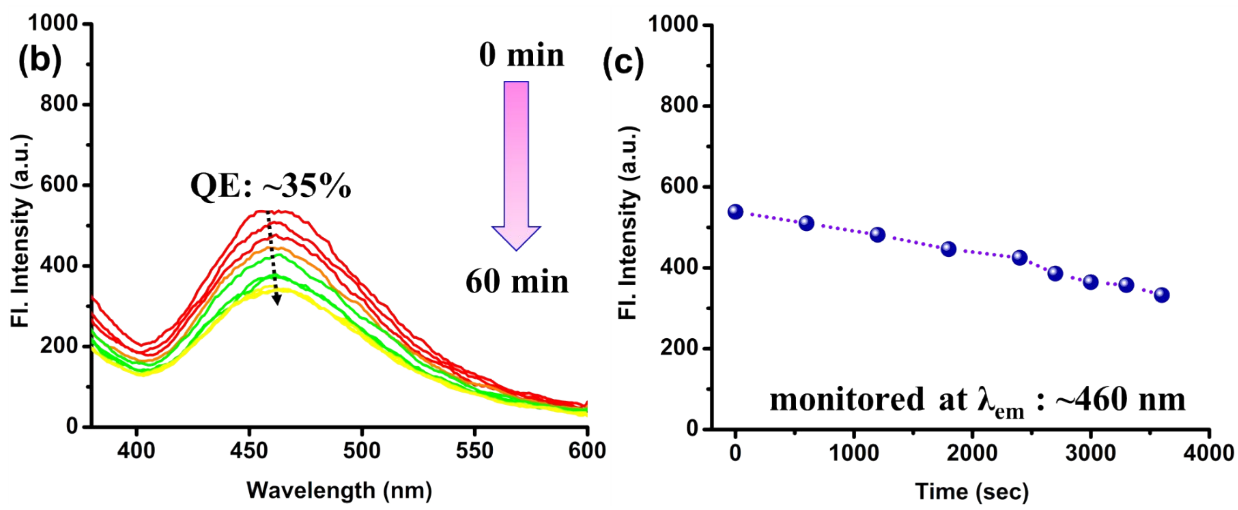

Fig. S43 (a) CP **2** drop-casted on a quartz slide for executing acetonitrile-mediated TNP vapour sensing study [left to right: front and perspective view under normal light and UV-torch]; (b) Fluorescence quenching (~35%) of CP **2** upon exposure of TNP (acetonitrile) vapour (up to ~60 minutes); (d) alteration of Fl. intensity as a function of elapsed time (monitored at ~460 nm).

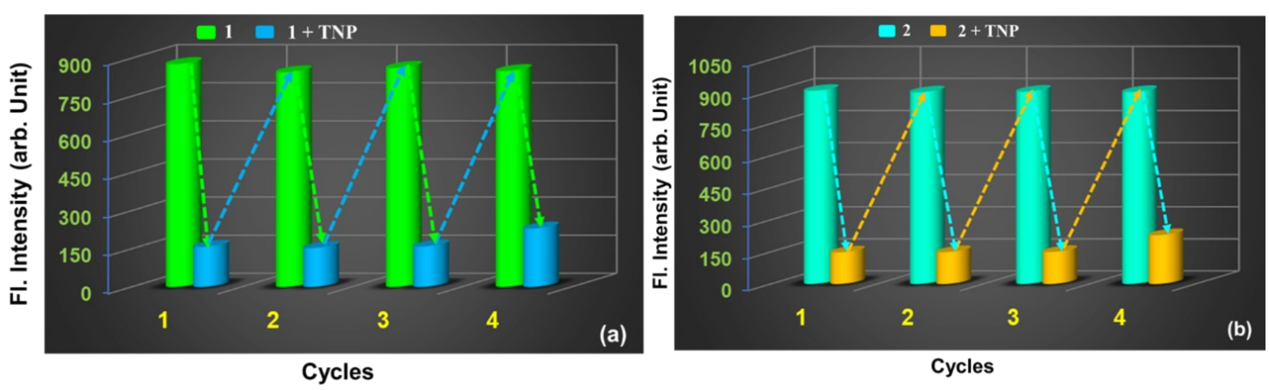

Fig. S44 Three times recyclable behaviour of the sensors **1** (a) and **2** (b) towards TNP sensing

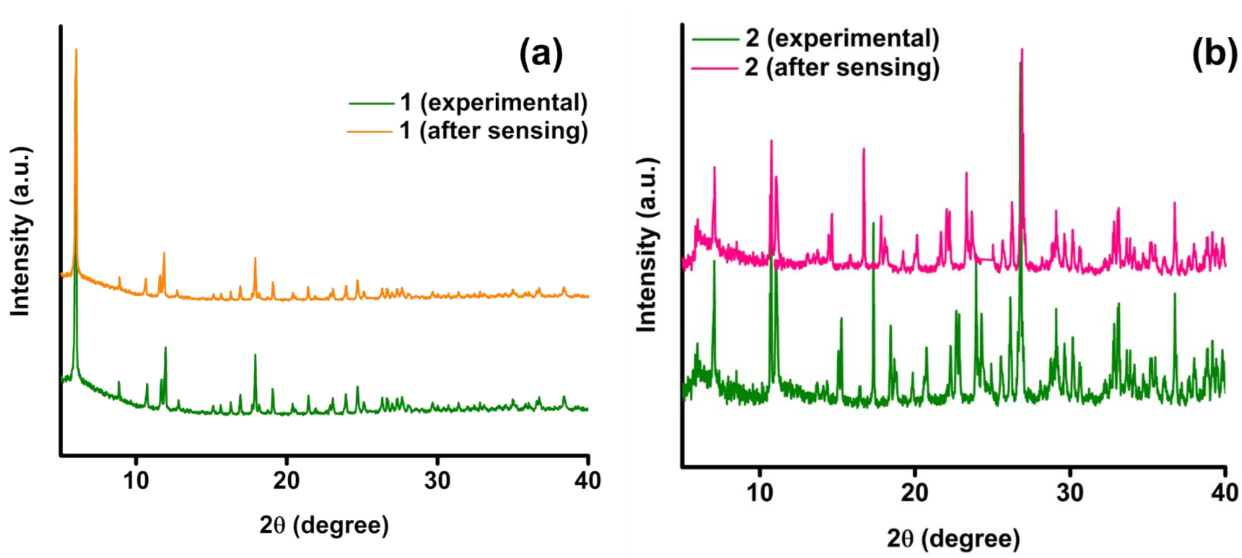

Fig. S45 Powder XRD pattern of **1** and **2**, before and after TNP sensing experiments; affirming no structural breakdown.

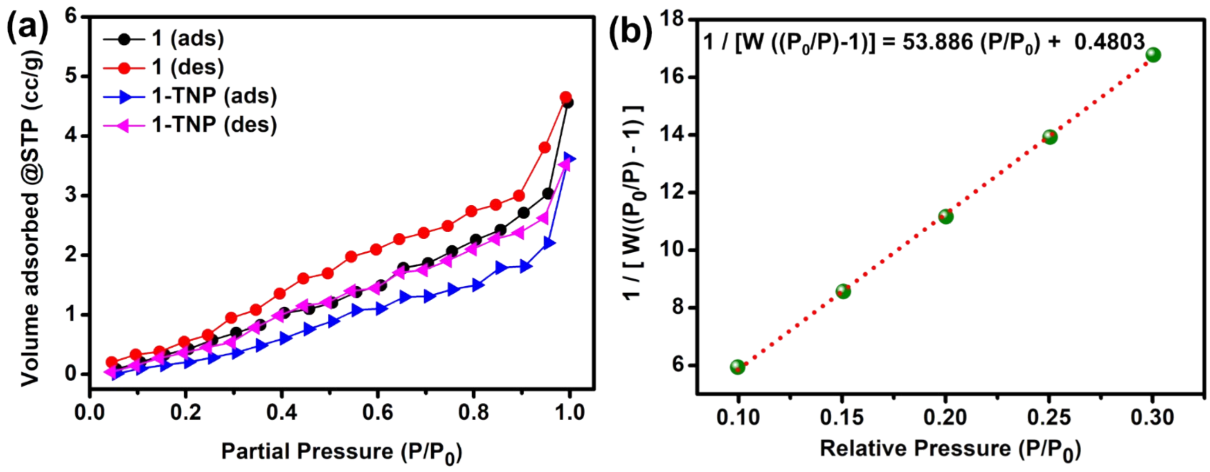

Fig. S46. (a) N_2 adsorption-desorption isotherm of **1** before and after TNP sensing study, (b) linear fitting of BET equation at low P/P_0 range for the isotherm obtained for **1**, depicting a surface area of 11.07 m^2/g.

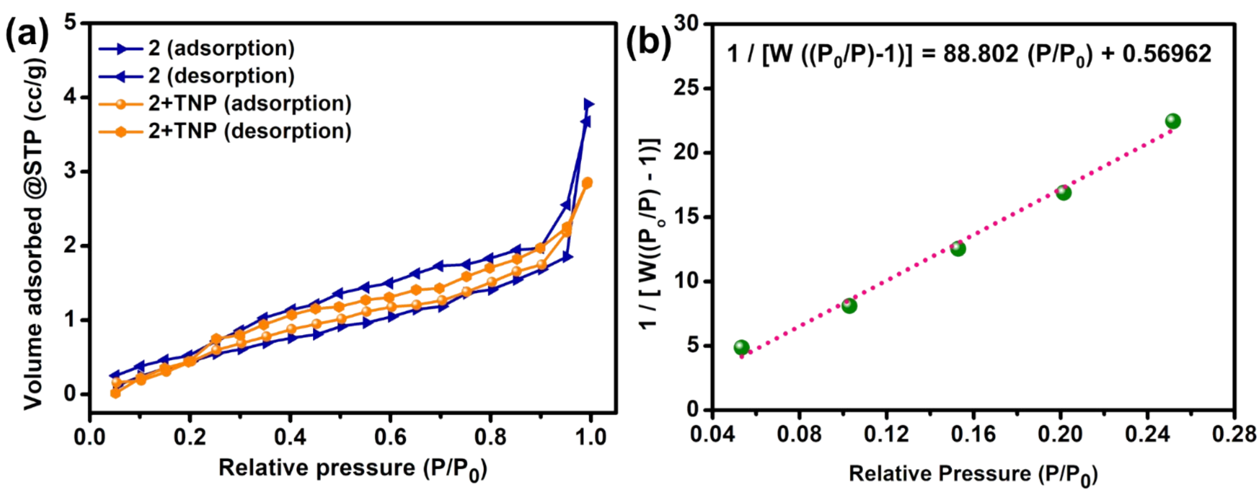

Fig. S47. (a) N_2 adsorption-desorption isotherm of **2** before and after TNP sensing study, (b) linear fitting of BET equation at low P/P_0 range for the isotherm obtained for **2**, depicting a surface area of 8.62 m^2/g.

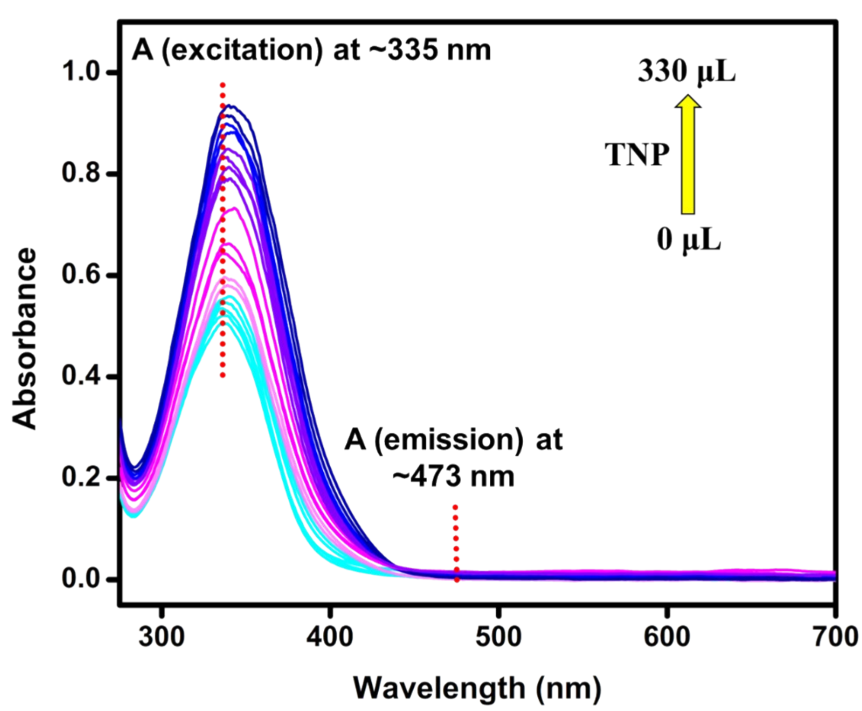

Fig. S48. Absorption spectra of **1** during gradual addition of TNP (10^{-4} M, in H_2O) for calculation of Inner Filter Effect (IFE) contribution.

Table S3 Calculation of IFE% of analyte (TNP) on the fluorescence profile of CP **1**/acetonitrile dispersion

Sl. No.	Analyte added (µL)	A_{ex}	A_{em}	I_{obs}	I_{corr}	I_{corr}/I_{obs} (correction factor, CF)	OE_{obs} (%)	OE_{corr} (%)
1.	0	0.5041	0.0009	940.02	1681.27	1.789	0	0
2.	10	0.5191	0.0019	884.84	1611.99	1.822	5.8700	4.120
3.	10	0.5342	0.0023	823.65	1527.54	1.855	12.379	9.144
4.	10	0.5442	0.0026	725.06	1360.74	1.877	22.868	19.065
5.	10	0.5518	0.0029	646.87	1225.09	1.894	31.186	27.133
6.	15	0.5693	0.0032	612.87	1184.73	1.933	34.802	29.534
7.	15	0.5919	0.0041	568.68	1129.45	1.986	39.503	32.821
8.	15	0.6421	0.0047	524.48	1104.41	2.106	44.205	34.311
9.	20	0.6547	0.0057	490.48	1049.12	2.139	47.822	37.600
10.	20	0.7099	0.0061	456.49	1040.95	2.280	51.438	38.085
11.	25	0.7827	0.0072	429.29	1065.86	2.483	54.331	36.604
12.	25	0.7952	0.0078	391.91	987.84	2.521	58.308	41.244
13.	25	0.8278	0.0086	357.89	937.45	2.619	61.927	44.241
14.	25	0.8354	0.0127	327.30	868.95	2.655	65.182	48.316
15.	25	0.8605	0.01384	279.71	765.38	2.736	70.244	54.476
16.	25	0.8831	0.0144	232.11	652.29	2.810	75.308	61.202
17.	25	0.9081	0.0152	198.12	573.56	2.895	78.924	65.885
18.	30	0.9207	0.0159	174.32	512.45	2.939	82.094	70.569

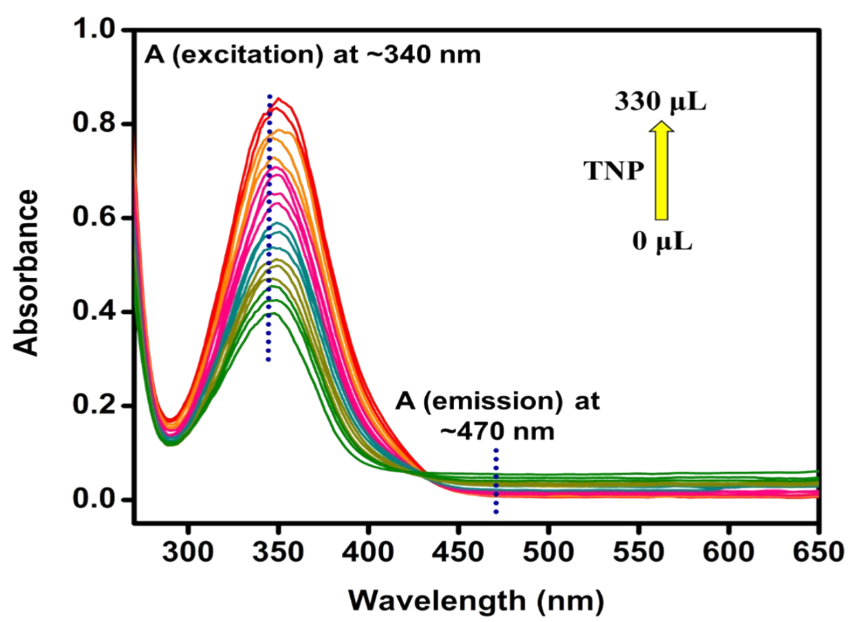

Fig. S49 Absorption spectra of **2** during gradual addition of TNP (10^{-4} M, in H_2O) for calculation of IFE contribution.

Table S4 Contribution of IFE% of analyte (TNP) on the fluorescence profile of CP **2**/acetonitrile dispersion

Sl. No.	Analyte added (μL)	A_{ex}	A_{em}	I_{obs}	I_{corr}	I_{corr}/I_{obs} (correction factor, CF)	OE_{obs} (%)	OE_{corr} (%)
1.	0	0.3855	0.0548	964.49	1601.208	1.660	0	0
2.	10	0.4144	0.0467	921.88	1567.561	1.700	4.418	2.101
3.	10	0.4354	0.0411	829.55	1435.795	1.731	13.991	10.330
4.	10	0.4633	0.0362	754.98	1341.793	1.777	21.722	16.201
5.	10	0.4748	0.0338	683.97	1228.392	1.796	29.085	23.283
6.	15	0.4959	0.0318	637.8	1170.940	1.836	33.872	26.871
7.	15	0.5221	0.0299	570.34	1076.797	1.888	40.866	32.751
8.	15	0.5432	0.022	541.93	1038.827	1.917	43.812	35.122
9.	20	0.5616	0.0196	520.62	1016.532	1.953	46.021	36.515
10.	20	0.5905	0.0182	481.56	970.511	2.015	50.071	39.389
11.	25	0.6168	0.0162	424.75	880.305	2.073	55.961	45.022
12.	25	0.6457	0.0128	392.78	838.300	2.134	59.276	47.646
13.	25	0.6746	0.0119	360.83	795.340	2.204	62.589	50.329
14.	25	0.6983	0.01	325.32	735.294	2.260	66.270	54.079
15.	25	0.7298	0.0096	289.81	678.911	2.343	69.952	57.600
16.	25	0.7535	0.0092	251.4	604.944	2.406	73.934	62.220
17.	25	0.7876	0.0083	208.2	520.512	2.500	78.413	67.493
18.	30	0.8087	0.0077	156.06	399.477	2.560	83.819	75.051

Table S5 HOMO, LUMO energies, orbital images of the NACs, CPs (**1** and **2**), its fluorophoric unit (HL), Sensor (1/2)•••analyte(TNP) adducts [from DFT calculations (B3LYP-level), performed using Turbomole (v7.0) software]. (Colour codes: Sea Green – C, Black – Cd, Red – O, Blue – N, White – H, Bright Yellow – S)

Entry	LUMO (eV)	HOMO (eV)	ΔE & Total Energy
HL	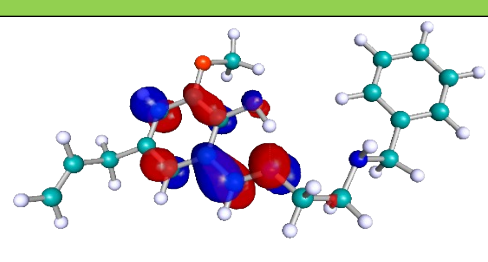 E_{LUMO} = - 1.412 eV	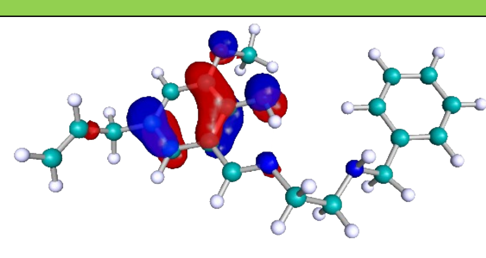 E_{HOMO} = - 5.807 eV	4.396 eV, T.E.: - 1035.05 KJ/mol

1	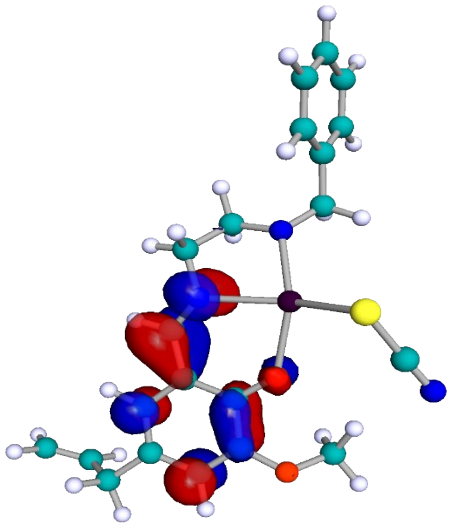 E_{LUMO} = - 1.012 eV	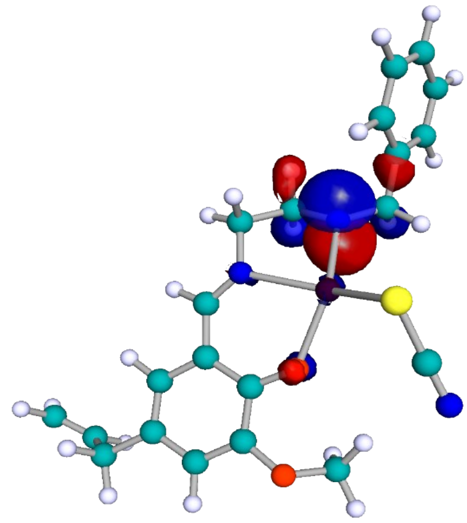 E_{HOMO} = - 4.552 eV	3.535 eV, T.E.: -1692.49 KJ/mol
2	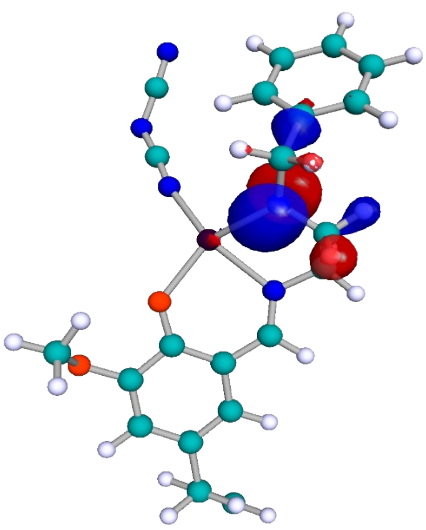 E_{LUMO} = - 3.21 eV	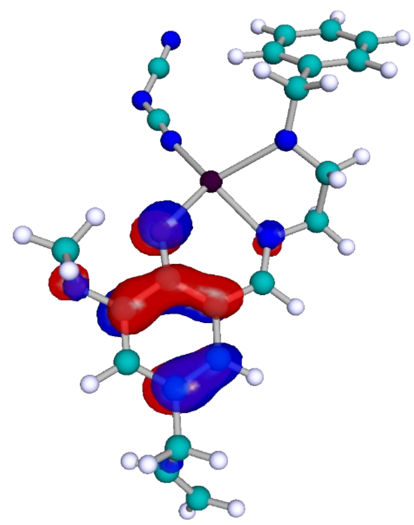 E_{HOMO} = -5.445 eV	1.935 eV, T.E.: -1441.721 KJ/mol
TNP	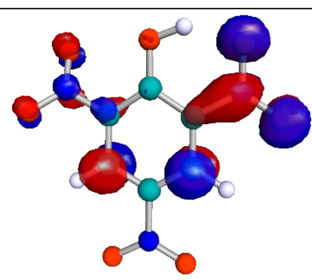 E_{LUMO} = - 3.374 eV	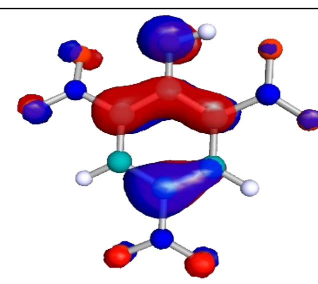 E_{HOMO} = - 7.728 eV	4.354 eV, T.E.: -919.85 KJ/mol
2,4-DNP	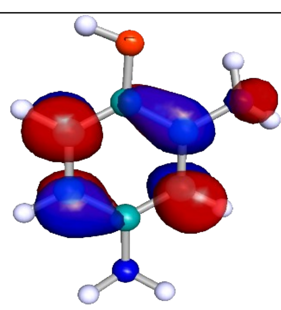 E_{LUMO} = -3.015 eV	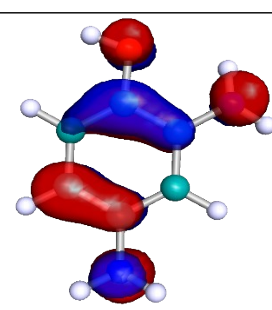 E_{HOMO} = - 7.26 eV	4.245 eV, T.E.: -715.60 KJ/mol

2,4-DNT	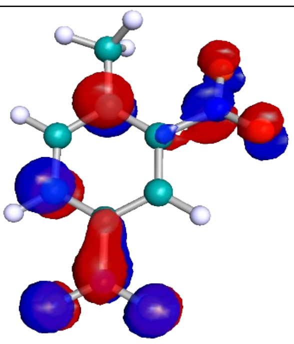 E_{LUMO} = -2.828 eV	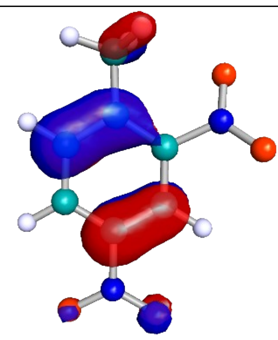 E_{HOMO} = - 7.763 eV	4.936 eV, T.E.: -679.71 KJ/mol
2,6-DNT	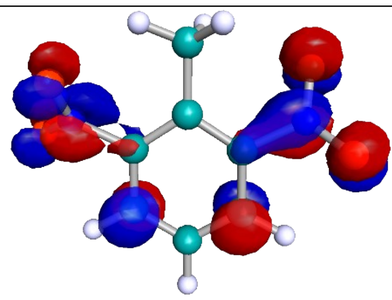 E_{LUMO} = -2.712 eV	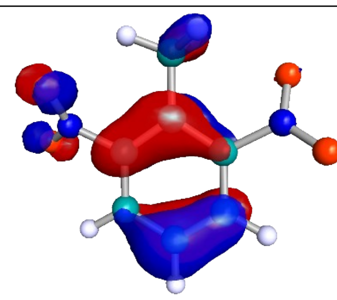 E_{HOMO} = - 7.636 eV	4.921 eV, T.E.: -679.70 KJ/mol
4-NP	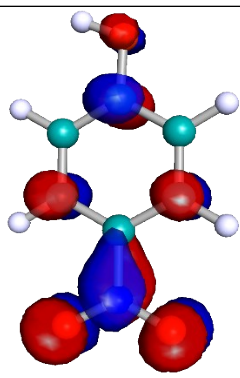 E_{LUMO} = -2.395 eV	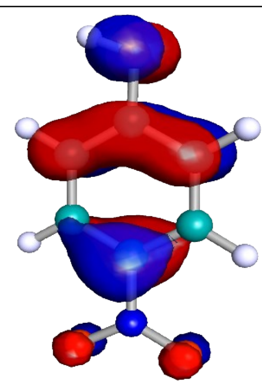 E_{HOMO} = -6.762 eV	4.365 eV, T.E.: -511.33 KJ/mol
1,3-DNB	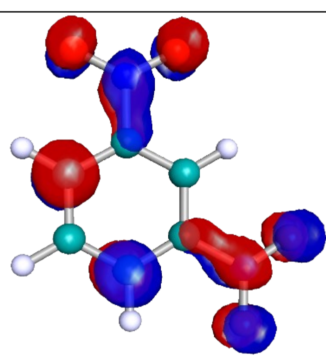 E_{LUMO} = -2.933 eV	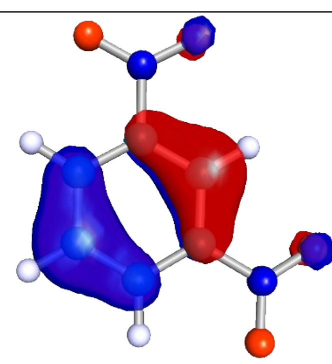 E_{HOMO} = -8.014 eV	5.080 eV, T.E.: -640.46 KJ/mol
2,4-DNA	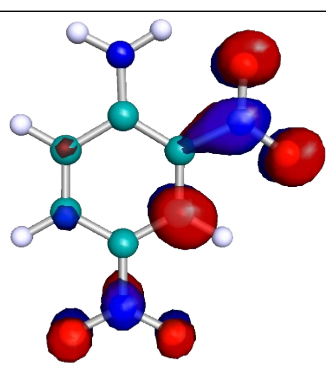	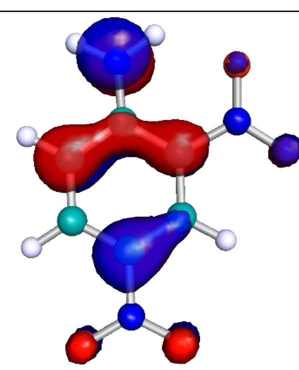	3.835 eV, T.E.: -695.76 KJ/mol

	E_{LUMO} = -2.678 eV	E_{HOMO} = -6.514 eV	
2,6-DNP	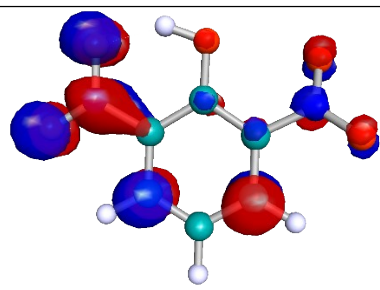 E_{LUMO} = -3.091 eV	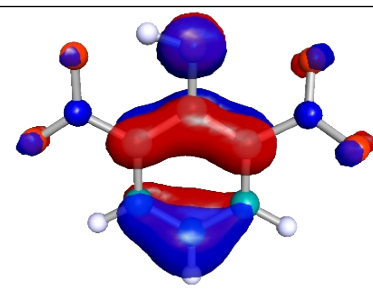 E_{HOMO} = -7.197 eV	4.107 eV, T.E.: -715.59 KJ/mol
4-NBA	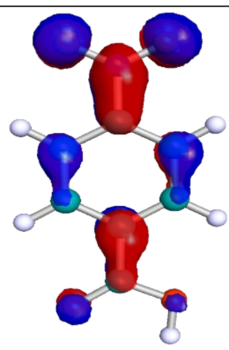 E_{LUMO} = -2.903 eV	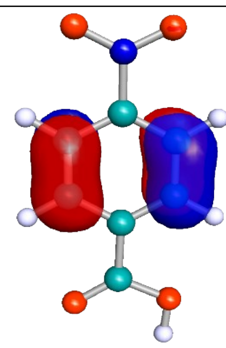 E_{HOMO} = -7.663 eV	4.759 eV, T.E.: -624.55 KJ/mol
3,5-DNBA	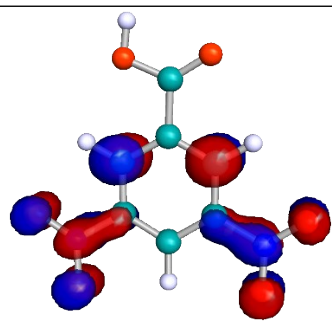 E_{LUMO} = -3.059 eV	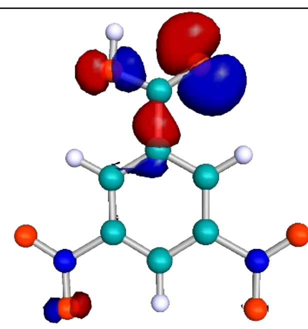 E_{HOMO} = -8.193 eV	5.137 eV, T.E.: -828.811 KJ/mol
NB	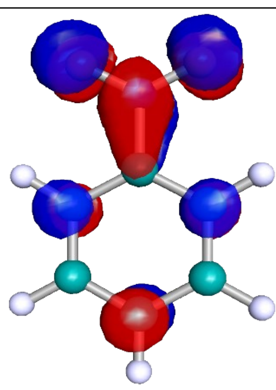 E_{LUMO} = -2.571 eV	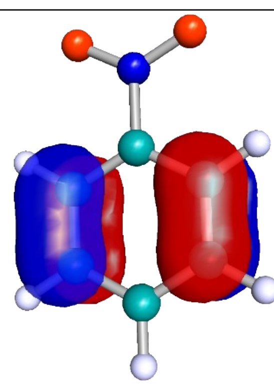 E_{HOMO} = -7.459 eV	4.887 eV, T.E.: -436.193 KJ/mol
HL + TNP	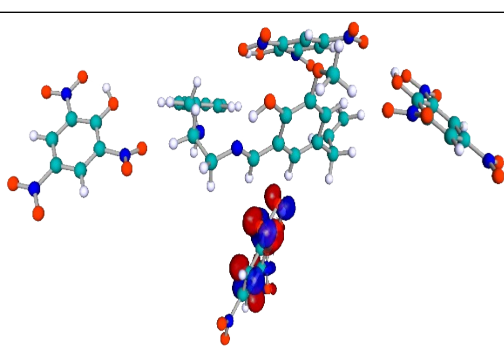	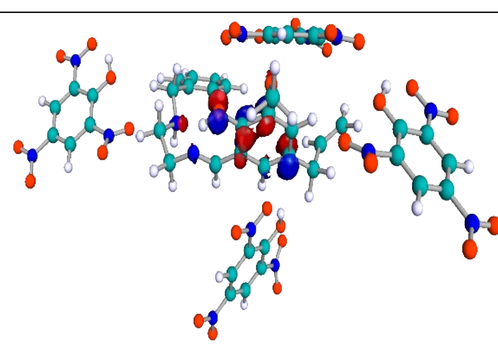	2.34 eV, T.E.: -4714.47 KJ/mol

	E_{LUMO} = -3.45 eV	E_{HOMO} = -5.79 eV	
1 + TNP	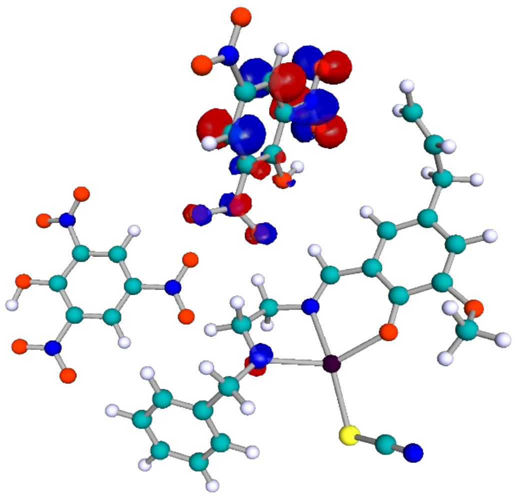 E_{LUMO} = -3.499 eV	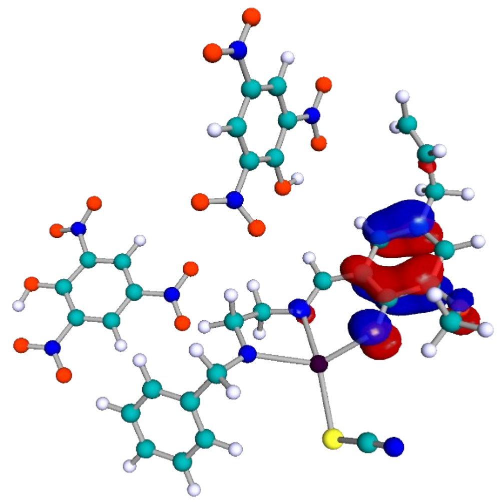 E_{HOMO} = -5.328 eV	1.836 eV, T.E.: -3532.059 KJ/mol
2 + TNP	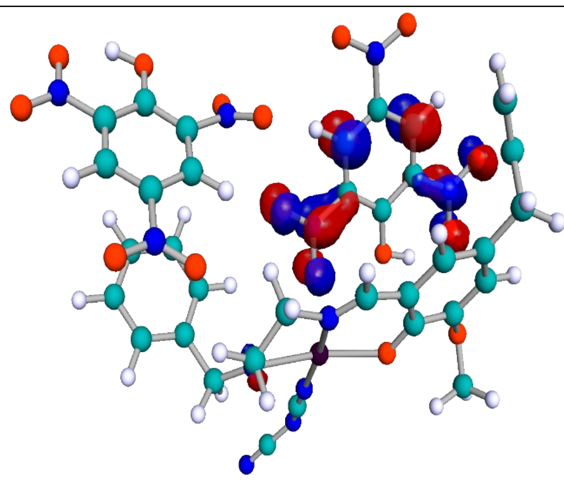 E_{LUMO} = -3.717 eV	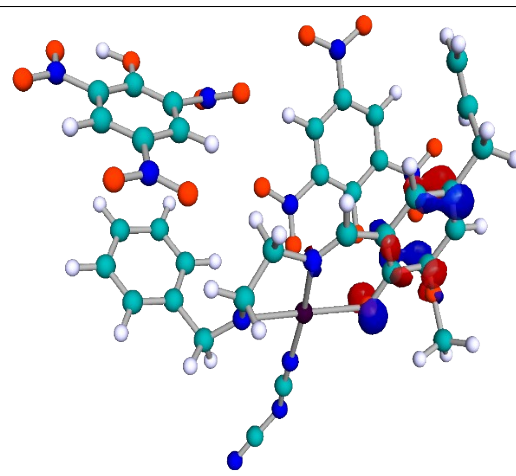 E_{HOMO} = -5.429 eV	1.713 eV, T.E.: -3281.43 KJ/mol

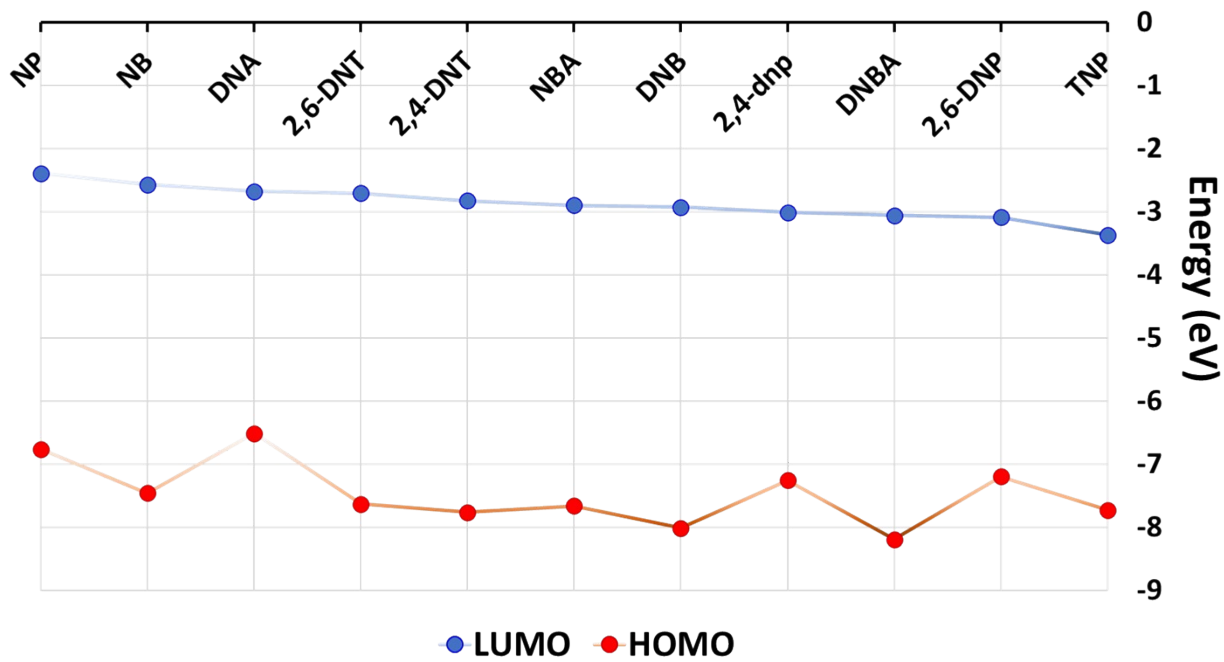

Fig. S50 Graphical depiction of comparative HOMO, LUMO energy levels of nitro-analytes.

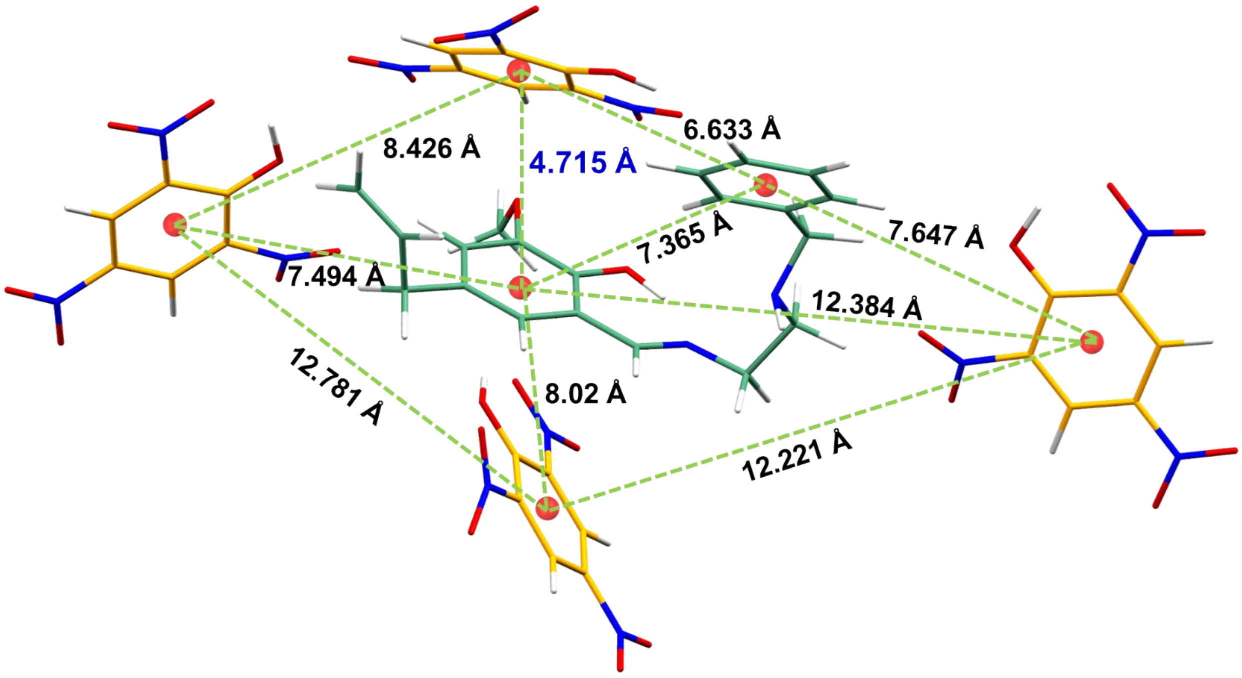

Fig. S51 Possibility of supramolecular π-π interaction, observed from geometry optimized structure of the HL•••TNP adduct (obtained from DFT Calculations)

Table S6 Preparation of complex environmental matrices (CEMs): real-field applications

(a) **Matchstick powder solution (MSPS)**: A few Matchsticks were collected from locally available match box, and the sticks were ground by mortar-pestle into a fine powder. It was sonicated in water for ~10-12 minutes. The as-obtained dispersion was passed through a normal filter paper and the filtrate was consequently utilized for preparing the simulated 10^{-4} M TNP solution (MSPS).

(b) **River water (RW)**: Water sample was collected from river Mayurakshi, near Suri, West Bengal, India. The water sample was used as it as to prepare a 10^{-4} M TNP solution (RW).

(c) **Sewage Water (SW)**: This water specimen was collected from the inlet of the Aqua Rejuvenation Plant (ARP) installed at CSIR-CMERI residential colony (~23.5449° N, 87.2918° E). The sample was filtered through a normal filter paper to screen out any macroparticles and the filtrate was used to prepare the simulated TNP solution.

(d) **Soil Sample Supernatant (SSS)**: The soil sample was collected from Tilpara Mihirlal Barrage, at Mayurakshi river basin, Suri, West Bengal, India. The laterite-based sandy soil sample was dried under sun for sufficient time, finely ground and ~5g of it was stirred in water for ~15-20 mins, followed by centrifuging for another ~10 min at ~3500 rpm. The supernatant (liquid) was accordingly used for preparation of the simulated TNP solution.

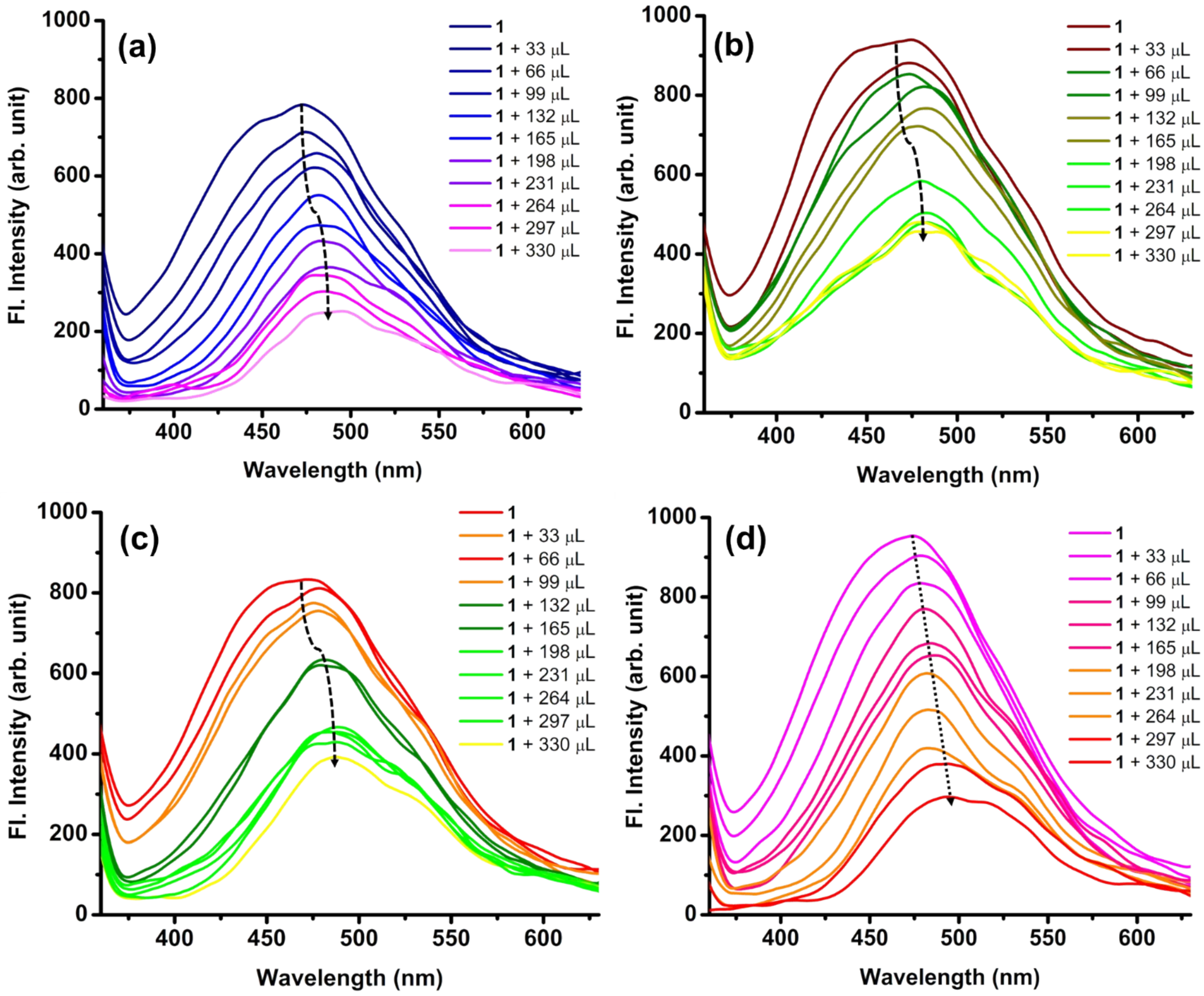

Fig. S52 Fluorescence Quenching of **1** during incremental addition of 10^{-4}(M) TNP at diverse complex matrices: (a) Matchstick powder solution (MSPS); (b) River Water (RW); (c) Sewage water (SW) and (d) Soil sample supernatant (SSS).

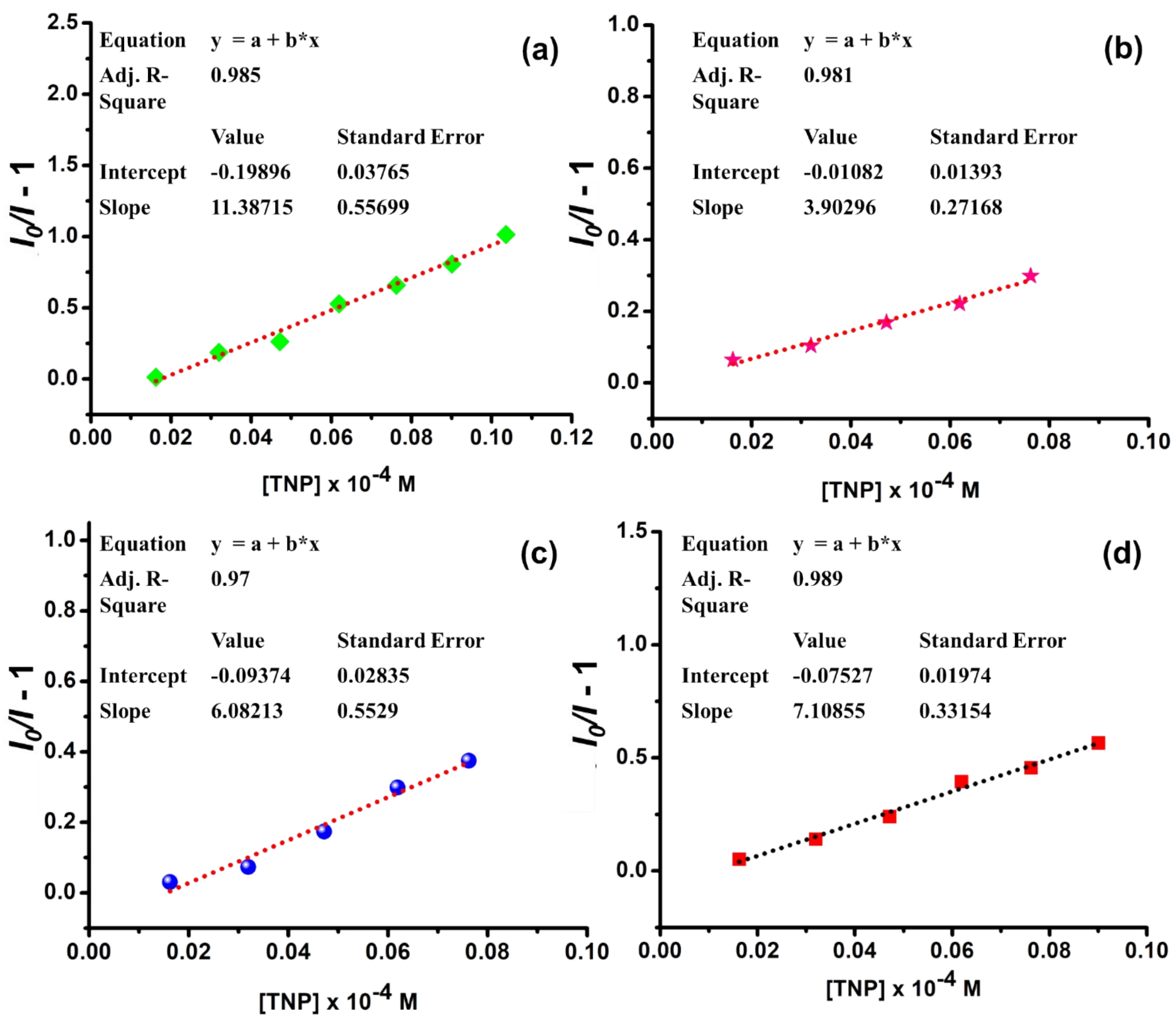

Fig. S53 Linear range of (I_0/I - 1) vs Concentration plot for calculation of K_{SV} as obtained from Figure S51 during fluorescence Quenching of **1** by complex environmental matrices: (a) MSPS; (b) RW; (c) SW and (d) SSS.

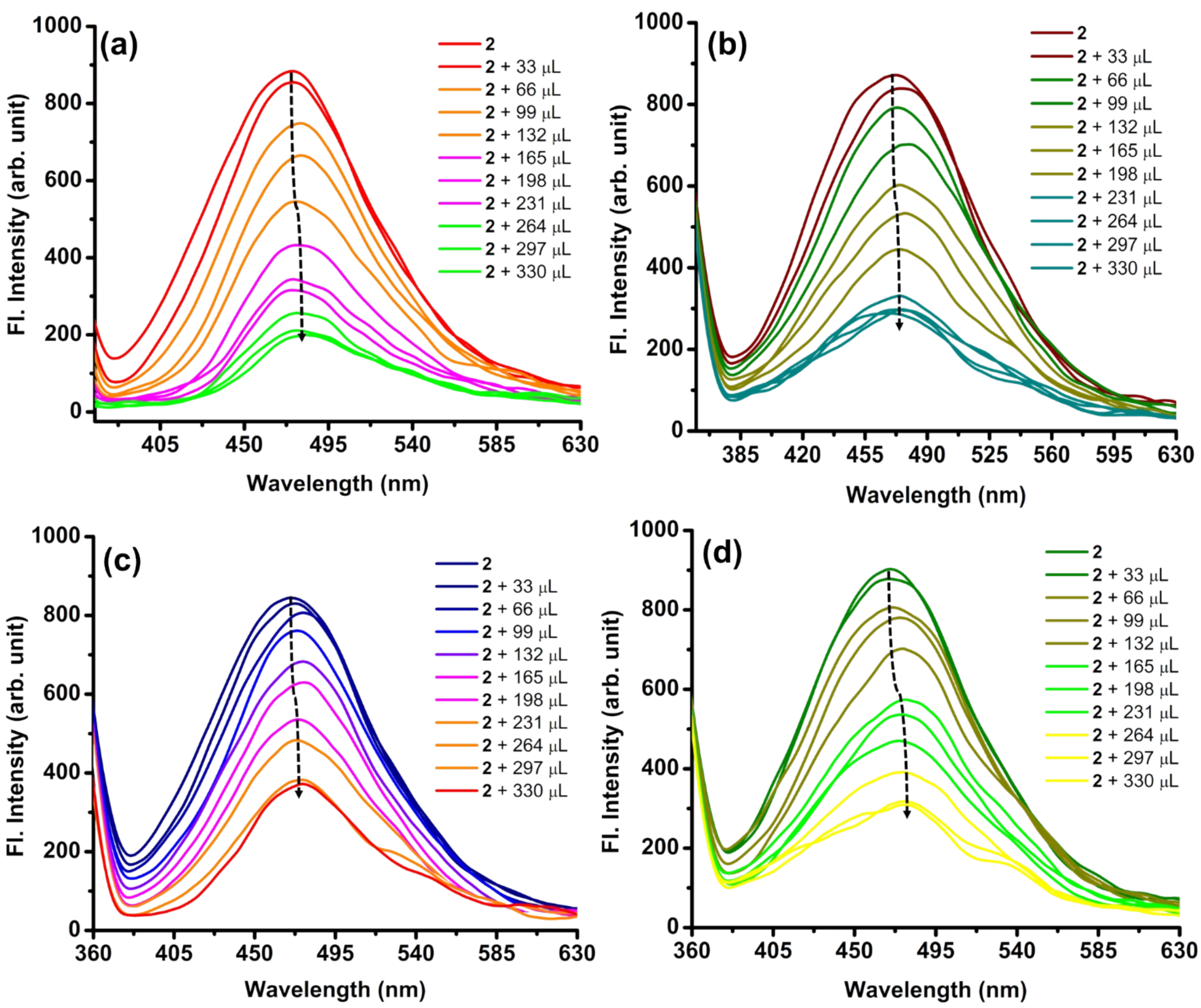

Fig. S54 Fluorescence Quenching of **2** during incremental addition of 10^{-4}(M) TNP at diverse complex matrices: (a) MSPS; (b) RW; (c) SW and (d) SSS.

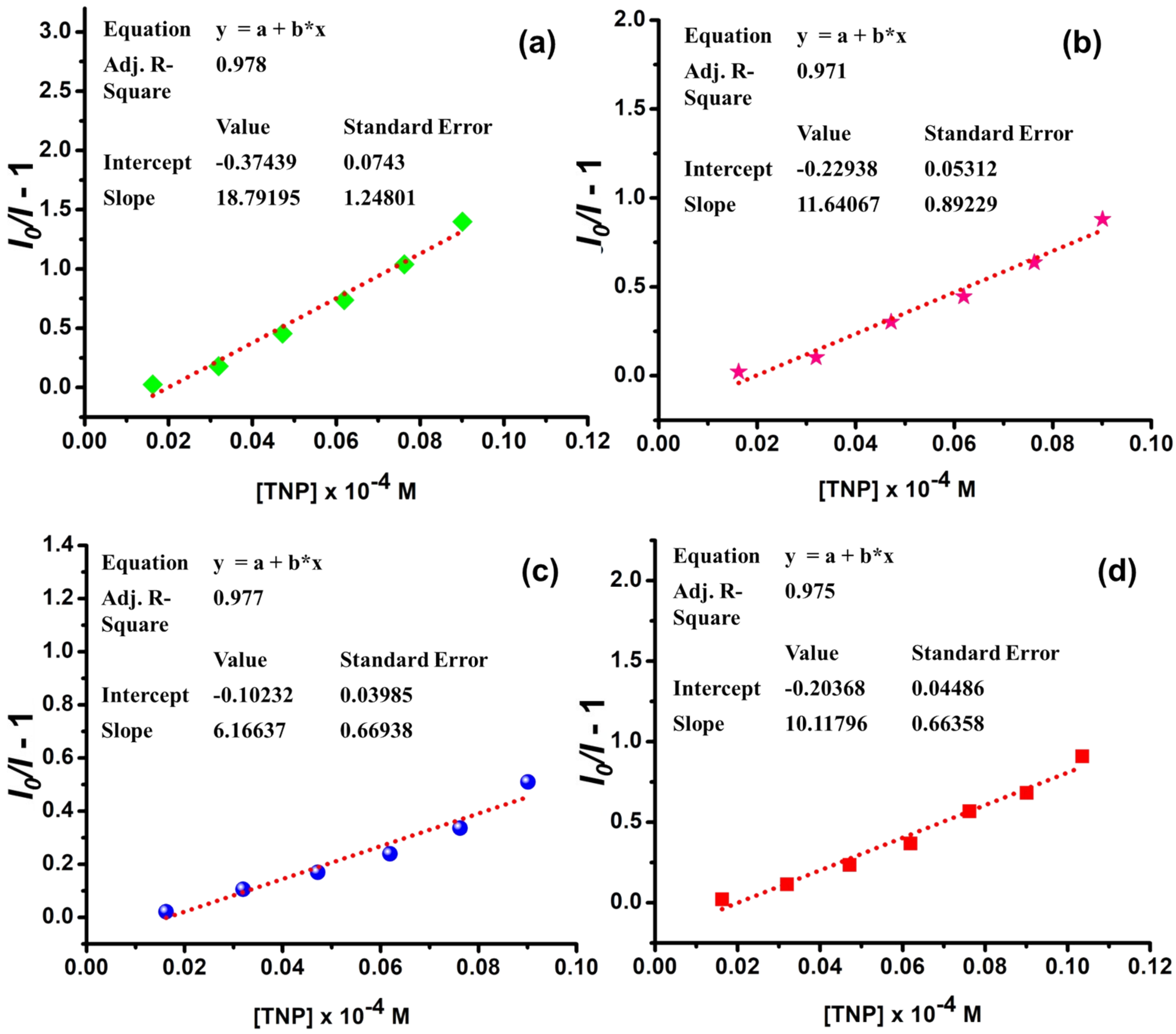

Fig. S55 Linear range of (I_0/I - 1) vs Concentration plot for calculation of K_{SV} as obtained from Figure S53 during fluorescence Quenching of **2** by complex environmental matrices: (a) MSPS; (b) RW; (c) SW and (d) SSS.

Table S7 Crystal parameters and selected refinement details for CPs **1** and **2**

Complex	**1**	**2**
CCDC	2314429	2314430
Empirical formula	$C_{21}H_{23}Cd_1N_3O_2S_1$	$C_{44}H_{45}Cd_2N_{10}O_4$
Formula weight	493.88	1002.72
Temperature (K)	200	273
Crystal system	Monoclinic	Monoclinic
Space group	$P2_1/c$	$P2_1/n$
a (Å)	14.9384 (3)	14.4942(9)
b (Å)	13.4833 (2)	10.3261(7)
c (Å)	10.6204 (18)	15.7836(10)
α(°)	90	90
β(°)	97.8443 (16)	115.732(2)
γ(°)	90	90

Volume (Å^3)	2119.14 (7)	2128.0(2)
Z	4	4
D_{calc} (g cm^{-3})	1.548	1.565
Absorption coefficient (mm^{-1})	9.343	1.054
F(000)	1000.0	1014.0
θ Range for data collection (°)	4.415 -77.473	1.972-27.159
Reflections collected	14048	58632
Independent reflection / R_{int}	4392/0.0583	4713/0.0615
Data / restraints / parameters	4392/0/ 254	4713 /0/ 281
Goodness-of-fit on F^2	1.044	1.096
Final indices[I>2σ(I)]	R1= 0.0337 wR1= 0.0859	R1= 0.0293 WR1= 0.0585
R indices (all data)	R1= 0.0381 wR2= 0.0888	R1= 0.0385 WR1= 0.0635
Largest diff. peak / deepest hole (e Å^{-3})	0.659/ -1.011	0.522 / -0.463

Table S8 Selected Bond lengths (Å) and Bond angles (°) for CPs **1** and **2**

1		**2**	
Atoms	**Distance (Å)**	**Atoms**	**Distance (Å)**
Cd1–N1	2.299(2)	Cd1-N1	2.331(2)
Cd1–N2	2.343(2)	Cd1-N2	2.346(2)
Cd1–N3	2.242(3)	Cd1-N3	2.266(2)
Cd1–O1	2.2467(18)	Cd1-N5	2.387(3)
Cd1–S2	2.7440(9)	Cd1-O1	2.2467(17)
Cd1–O1(1)	2.3623(19)	Cd1-O1(1)	2.3233(17)
Atoms	**Angle (º)**	**Atoms**	**Angle (º)**
N2–Cd1–N1	75.52	N1–Cd1–N2	74.45
N1–Cd1–O1	79.14	N1–Cd1–N5	85.59
O1–Cd1–O1(1)	82.31	N5–Cd1–N2	101.74

O1–Cd1–N2	84.46	O1–Cd1–O1(1)	78.42
O1–Cd1–N3	90.28	N1–Cd1–O1	78.43
N3–Cd1–S2	83.14	N2–Cd1–O1	91.13
S2–Cd1–N1	93.22	N3–Cd1–O1	102.49
N3–Cd1–N2	112.14	N5–Cd1–O1	89.67
Cd1–O1–Cd1	97.69(7)	Cd1–O1–Cd1	101.57(6)

Table S9 Comparison table: recently reported CP-based chemosensors towards TNP detection.

Entry	Compound	Detection Medium	Analytical Parameters		Vapour phase sensing	References
			LOD **(μM)**	K_{SV} **(M^{-1})**		
1.	[Cd(NDI-A)(seb)(H_2O)]	EtOH	0.814	4.75 × 10^4	No	*Inorg. Chem.*, 2022, **61**, 26, 10066-10078
2.	[Cd(INA)(pytpy)(OH)]· 2H_2O	DMF	2.41	4.3×10^4	No	*Sens. Actuators B Chem.*, 2018**, 272**, 166-174
		H_2O	9.1	3.3×10^4		
3.	[Zn_2Na_2-(TPHC)(4,4-Bipy)(DMF)]·8H_2O	DMF	0.64	8.47×10^4	No	*Inorg. Chem.*, 2019**, 58**, 4026-4032
4.	[Pb_7(TTPCA)$_4$$Cl_2$]·3$H_2O$	H_2O	1.03	5.22 × 10^4	No	*Inorg. Chem.*, 2021,**60**, 7887-7899
5.	[Pb_7(TTPCA)$_4$(DMA)$_2$ (HCOO)$_2$].H_2O	H_2O	1.03	4.33×10^4	No	
6.	[Pb_4(TTPCA)$_3$]·3DMF· 2H_2O·H_3O	H_2O	2.63	3.14×10^4	No	
7.	[Eu_2(1,4-NDC)$_3$(DMF)]$_n$ (2-Eu)	H_2O	0.89	6.98× 10^4	No	*Cryst. Growth Des.*, 2021, **21**, 6543-655
8.	[Cd(L1)(N(CN)$_2$)]$_n$ (Compound 1)	H_2O	0.68	7.49× 10^4	Yes	*Inorg. Chem.*, 2023, **62**, 1, 98-113
9.	[Cd(L1)(NCS)]$_n$ (Compound 2)	H_2O	0.41	8.01× 10^4	Yes	
10.	[Cd_2(L2)$_2$(NCS)$_2$)]$_n$ (Compound 3)	H_2O	1.18	8.10× 10^4	Yes	
11.	[Zn-(PBBA)(H_2O)]· 3DMF·2H_2O	H_2O	1.00	4.4 × 10^4	No	*Inorg. Chem.*, 2023, **62**, 1272-1278
12.	[Zn_2(NO_3)$_2$(4,4'-bpy)$_2$(TBA)]	H_2O	6.02	4.83×10^4	No	*CrystEngComm*, 2019, **21**, 1948-

						1955
13.	$\{[Zn(L)(H_2O)_2]\cdot H_2O\}$ and $\{[Cd(L)(H_2O)_2]\cdot 4H_2O\}_n$	H_2O	0.63 and 0.75	9.77×10^4 and 8.52×10^4	No	*CrystEngComm*, 2019, **21**, 5185-5194
14.	$\{[Zn(mbhna)(bpma)]\}_n$	H_2O + MeOH	5.89	7.8×10^3	No	*Dye. Pigment.*, 2023, **210**, 111025
15.	$\{[Cd\ (mbhna)(bpma)].DMF\}_n$	H_2O + MeOH	2.29	1.09×10^4	No	
16.	$\{[Zn(mbhna)(bpea)]\}_n$	H_2O + MeOH	2.59	1.17×10^4	No	
17.	$\{[Cd(mbhna)\ (bpea)]\}_n$	H_2O + MeOH	2.80	8.9×10^3	No	
18.	$\{[Zn(mbhna)(bpta)]\}_n$	H_2O + MeOH	4.80	1.7×10^4	No	
19.	$\{[Cd(mbhna)(bpta)(CH_3OH)]\}_n$	H_2O + MeOH	2.06	1.6×10^4	No	
20.	$\{[Zn(mbhna)(bpba)].CH_3OH\cdot H_2O\}_n$	H_2O + MeOH	1.72	1.44×10^4	No	
21.	$\{[Cd(mbhna)(bpba)]\}_n$	H_2O + MeOH	1.05	2.84×10^4	No	
22.	$\{[Cd_4(L)_2(L_2)_3(H_2O)_2](8DMF)(8H_2O)\}_n$	Ethanol	4.90	3.89×10^4	No	*Inorg. Chem.*, 2016, **55**, 1741-1747
23.	$Zn_2(TZBPDC)(\mu_3\text{-}OH)(H_2O)_2$	H_2O	278.00	4.90×10^4	No	*Chem. Commun.*, 2016, **52**, 5734-5737
24.	$[(CH_3)_2NH_2]_3[Zn_4Na(BPTC)_3]\cdot 4CH_3OH\cdot 2DMF$	H_2O	5.00	3.2×10^4	No	*J. Mater. Chem., A.* 2015, **3**, 7224-7228
25.	$\{[Cd_3(bmipia)_2]\cdot 10DMF\cdot 5H_2O\}_n$	H_2O	NA	3.82×10^4	No	*Cryst. Growth Des.*, 2020, **20**, 1373-1377
26.	$[\{Cd(fdc)(bpee)_{1.5}\}.3(H_2O)]$	EtOH	5.00	6.64×10^4	No	*Cryst. Growth Des.*, 2015, **15**, 3356−3365
27.	$\{[Cd_2(tdz)_2\ (4,4'\text{-}bpy)_2]\cdot 6.5H_2O\}_n$	H_2O	6.30	4.86×10^4	No	*Dalton Trans.*, 2019, **48**, 2388
28.	$\{[Cd(L_1)(L_2)](DMA)\}_n$ (Cd-MOF1)	H_2O	7.03	NA	No	*New J. Chem.*, 2022, **46**, 8523-8533
29.	$[In(HTzPTpy)Cl_2]$	H_2O	1.31	8.95×10^4	No	*New J. Chem.*, 2022, **46**, 1551-

	(CUST-801)					1556
30.	$[Zn_3(Bip)_3(H_2sip)_2(H_2O)_4].5H_2O$	H_2O	54.40	3.44×10^4	No	*New J. Chem.*, 2022, **46**, 22739
31.	$[Cd(L1)(SCN)_2H_2O]_n$	H_2O	55	3.4×10^4	No	*Inorg. Chem.*, 2024, **63**, 4527–4544
32.	$[Cd_{1.5}(L1)(N(CN)_2)_3]_n$	H_2O	28	6.9×10^4	No	
33.	$[Cd(L2)(SCN)_2]_n$	H_2O	27	2.3×10^4	No	
34.	$[Cd_{1.5}(L2)(N(CN)_2)_3]_n$	H_2O	31	2.3×10^4	No	
35.	$[Cd_2(L_1)(NCS)_2(CH_3OH)]_n$	DMSO + Acetonitrile	1.33	$1.25x10^4$	No	*Cryst. Growth Des.*, 2019, **19**, 6431–6447
36.	$\{[Cd(HL_1)_2(N(CN)_2)_2].H_2O\}_n$	DMSO + Acetonitrile	0.33	$1.71x10^4$	No	
37.	$[Cd(HL_2)_2(N(CN)_2)_2]_n$	DMSO + Acetonitrile	0.16	$1.82x10^4$	No	
38.	$[Cd(L)(SCN)]_n$ (CP **1**)	H_2O	0.29	5.91×10^4	Yes	**Present work**
39.	$[Cd(L)(N(CN)_2)]$ (CP **2**)	H_2O	0.15	17.6×10^4	Yes	

[**Abbreviations**: NDI-A= N,N'-di(4-pyridylacylamino)-1,4,5,8-naphthalenediimide; seb = sebacic acid; INA = Isonicotinic acid; pytpy = 4'-(4-Pyridinyl)-2,2':6',2"-terpyridine; TPHC= [1,1′:2′,1″-terphenyl]-3,3″,4,4′,4″,5′-hexacarboxylic acid; 4,4-bipy= 4,4-bipyridine, DMF = N,N-dimethylformamide; H_3TTPCA = 1,1′,1″-(1,3,5-triazine-2,4,6-triyl)-tripiperidine-4-carboxylic acid; DMA = N,N-dimethylacetamide; 1,4-H_2NDC = 1,4-naphthalenedicarboxylic acid; HL1 (Entry 8, 9) = schiff based ligand from 3-Ethoxysalicylaldehyde and *N*-benzyl ethylenediamine; HL2 (Entry 10) = schiff based ligand from o-vanillin and *N*-benzyl ethylenediamine; PBBA = 4,4′-(2,6-pyrazinediyl)bis[benzoic acid]; H_2TBA= 4-(1H-tetrazol-5-yl)-benzoic acid; 4,4′-bpy = 4,4′-bipyridine; H_2L (Entry 13): 5-(4-pyridylamino)isophthalic acid; mbhna = 4,4′ -methylene-bis[3-hydroxy-2-naphthalene carboxylate; bpxa (Entry 14-21) = N,N′ -bis(pyridylmethyl)alkylamine with x = m (methyl), e (ethyl), t (tert-butyl) or b (benzyl); H_4L(Entry 22) = [1,1′:3′,1″-terphenyl]-4,4′,4″,6′-tetracarboxylic acid; L_2= 2-amino-4,4′-bipyridine; BPTC= biphenyl-3,3′,5,5′-tetracarboxylic acid; H_6bmipia: 5-[N,N-bis(5-methylisophthalic acid)amion] isophthalic acid; fdc = 2,5-furandicarboxylate dianion; bpee = 1,2-bis(4-pyridyl)ethylene; H_2tdz= thiadiazole dicarboxylate; L_1 (Entry 28) = 2-amino-1,4-benzenedicarboxylate; L_2 (Entry 28) = 4,4'-azopyridine; HTzPTpy = 4-(tetrazole-5-yl)phenyl-[2,2':6',2"]-terpyridine); Bip = 3,5-bis(imidazole-1-yl)pyridine; H_2sip = 5-sulfoisophthalic acid, L1(Entry 31,32) = schiff based ligand from 3-formylchromone and N,N-diethylethylenediamine, L2(Entry 33,34) = schiff based ligand from 3-formylchromone and N,N-dimethylethylenediamine, HL_1(Entry 35,36) = schiff based ligand from 3- aminoquinoline and o-vanillin, HL_2(Entry 37) = schiff based ligand from 5- aminoquinoline and o-vanillin]